For submission to Organic Geochemistry

Multi-spectroscopic and elemental characterization of southern Australian asphaltites

Alan G. Scarlett[a*], Alex I. Holman[a], Svetoslav V. Georgiev[b], Holly J. Stein[b,c], Roger E. Summons[d], and Kliti Grice[a*]

[a] Western Australian Organic and Isotope Geochemistry Centre, The Institute for Geoscience Research, School of Earth and Planetary Sciences, Curtin University, Western Australia

[b] AIRIE Program, Colorado State University, Fort Collins, 80523-1482 CO, USA

[c] Geosciences, University of Oslo, Norway

[d] Department of Earth, Atmospheric and Planetary Sciences, Massachusetts Institute of Technology, 77 Massachusetts Avenue, Cambridge, MA 02139, USA

Corresponding author: * alan.scarlett@curtin.edu.au, K.Grice@curtin.edu.au (post publication only)

Highlights

- GC×GC-TOFMS analyses shows asphaltene hydropyrolysates similar to maltenes
- Isoprenoids to *n*-alkanes δ^2H offsets suggest oil generation at low thermal maturity
- Carotenoid-derived hydrocarbons suggest persistent photic zone euxinia
- Concentrations of metal quantification indicates anoxic depositional environment
- Re-Os dating suggests asphaltites originate in Cretaceous (103 ± 22 Ma)

Abstract

Strandings of various types of bitumen along the coast of southern Australia are long known. Among these, brittle, angular lumps termed ‘asphaltites’ are possibly sourced from Cretaceous source rocks linked to an oceanic anoxic event (OAE), but the exact source remains unclear. The unusual chemical composition of these asphaltites and their survival during transport and shoreline stranding suggest that they formed by nearby submarine seepage of asphaltene-rich crude oils. Here, we provide a detailed organic and inorganic geochemical characterization of asphaltites to constrain their origin and age. High-pressure hydropyrolysis (HyPy) of asphaltene fractions from ten asphaltites releases similar assemblages of macromolecularly bound compounds, suggesting a common source for all asphaltites. Comprehensive gas chromatography–time-of-flight mass spectrometry (GC×GC-TOFMS) was used to compare these asphaltene-derived compounds with the maltene fractions, while compound specific isotope analysis (CSIA) was used to compare $\delta^{13}C$ and $\delta^{2}H$ of *n*-alkanes and isoprenoids. A large offset between the $\delta^{2}H$ of the *n*-alkanes and isoprenoids suggests oil generation and expulsion at low thermal maturity. The mean concentrations of isorenieratane and chlorobactane, carotenoid derivatives indicative of photic zone euxinia (PZE), in the asphaltites were 8.8 ± 0.8 SEM µg g^{-1} and 1.4 ± 0.1 SEM µg g^{-1}, respectively. A mean Aryl Isoprenoid Ratio of 0.75 (sd = 0.17) is accompanied by Pr/Ph of ~1.2. These features strongly support persistent PZE conditions at the level expected for an OAE. Trace metal contents of the asphaltites, including low selenium and high vanadium concentrations, also support anoxic conditions. Rhenium-osmium (Re-Os) analyses constrain the age of asphaltite generation to 103 ± 22 Ma, with relatively a low initial $^{187}Os/^{188}Os$ ratio of 0.44 ± 0.18. Integrating local geologic knowledge with organic and inorganic geochemistry and Re-Os isotopic results, we identify a Cretaceous unit associated with OAE1a (~125 Ma) as the most likely source of the asphaltites. Alternative scenarios involving source rocks deposited during OAE1b (~112 Ma) are possible, but require rapid burial of organic-rich sediments to reach required maturation levels in a shorter time.

Keywords

Re-Os geochronology; Isotopic composition; Solid bitumen; Oil seeps; Tar mats; Bight Basin

1. Introduction

Crude oil stranded along coastlines around the world can be the result of oil pollution or natural seepage. It has been estimated that natural marine seeps contribute about half of all oil inputs into the sea (NRC, 2003). Along a *ca* 1000 km stretch of the southern Australian coastline, coastal bitumens have been encountered since at least the early 19th century, and most are thought to originate from natural sources (reviewed by Edwards et al., 2016). A coastal bitumen survey in 1990 – 1991 classified one type of coastal bitumen as 'asphaltites' characterised as "black solid lumps which break with a subconchoidal to conchoidal fracture, exhibit a vitreous lustre and have a strong petroliferous odour" (Fig. S1), distinct from the waxy class of coastal bitumens also found during the survey (Edwards et al., 2016). The asphaltites are typically heavy (4 – 18° API), rich in sulphur (*ca* 4 %), and possess a large asphaltene content (42 – 84 %) (Edwards et al., 1998; Hall et al., 2014; Edwards et al., 2016). As the asphaltites are typically slightly denser than seawater they are likely to have spent significant time below the ocean surface, possibly on the seafloor as evidenced by the presence of various marine organisms on some of the asphaltites (Edwards et al., 2016). This class of asphaltite, termed 'Family 4' by Edwards et al. (1998), has been of considerable interest due to its unique composition compared with Australian crude oils and the potential for oil discovery in the Great Australian Bight.

To help constrain the source of the asphaltites, Hall et al. (2014) thoroughly reviewed the possible origins of the initially discharged asphaltic bitumen based upon the classification system described by Curiale (1986) that proposed a continuum from pre-oil (plastic extrusion from rich source rocks) to post-oil (alteration product of once liquid oil). The unusual characteristics of Family 4 asphaltites did not allow for any conclusive answer as to their

origin but Hall et al. (2014) suggested that the most likely mechanism was tar mat formation, probably caused by deasphalting, along a flat-lying migration pathway during secondary migration of the main oil stringer, or through deasphalting related to gas invasion of the reservoir. The study by Hall et al. (2014) showed that previously unanalysed samples could be correlated with the 'Family 4' asphaltites, based on their physical, molecular and compound-specific $\delta^{13}C$ isotopic signatures. The asphaltites showed little evidence of weathering or biodegradation although they did report some differences between the outer surface and inner section of the samples, and that this was dependant on the location of the collection site; it was noted that photo-oxidation may have contributed to this. The lack of biodegradation was evident from the prominent *n*-alkane distribution apparent in the Total Ion Chromatograms (TIC; Fig. 8A Hall et al. (2014)) of the saturated hydrocarbon fraction. There was, however, an underlying unresolved complex mixture (UCM) of hydrocarbons and therefore Hall et al. (2014) also carried out urea adduction to separate the *n*-alkanes from the branched/cyclic fraction. An alternative approach to dealing with the complexity of UCMs is to perform comprehensive gas chromatography – time-of-flight mass spectrometry (GC×GC-TOFMS) which provides enhanced chromatographic resolution and has been successfully used to more fully characterise oils (e.g. Frysinger et al., 2003; Arey et al., 2007; Booth et al., 2007; Ventura et al., 2008; Eiserbeck et al., 2012; Nelson et al., 2016). The use of GC×GC-TOFMS may therefore complement the previous characterisations of the 'Family 4' asphaltites.

It has been noted that the asphaltites possess a large asphaltene fraction (Hall et al., 2014; Edwards et al., 2016), representing a substantial proportion of the sample that has not been subjected to analysis. One way of gaining information from the asphaltene fraction is to perform high-pressure hydropyrolysis (HyPy) to release macromolecularly bound compounds trapped within the asphaltene matrix. The HyPy process involves the thermal decomposition of organic matter with increasing temperatures in the presence of hydrogen to characterise coals and oil shales (e.g. Bishop et al., 1998; Brocks et al., 2003; Sonibare et

al., 2009). An important attribute of HyPy cracking is the release of macromolecularly bound hydrocarbons with minimal isomeric alteration (Love et al., 1997). The use of HyPy can thus yield hydrocarbons similar to those of the original oil but not affected by secondary processes such as migration contamination, water washing and biodegradation. Therefore a more comprehensive profile of the asphaltites' origin may be produced from the suite of biomarkers present. The hydropyrolysates derived from the asphaltene (i.e. 'macromolecular' fraction) can then be compared with those of the maltene fraction, either by targeting specific biomarkers, such as carried out by Boreham et al. (2001) or by more general characterisation permitted by GC×GC-TOFMS, as conducted in this study.

It was noted by Totterdell and Mitchell (2009) that the asphaltites possess isorenieratane. Isorenieratane is a diagenetic product of the carotenoid isorenieratene, a pigment exclusively synthesized by specific brown-pigmented strains of green sulphur bacteria (Chlorobiaceae), and is indicative of anoxic and sulphidic conditions in the presence of light in planktonic environments - i.e. photic zone euxinia (PZE) (Grice et al., 1996; Brocks and Summons, 2004; Grice et al., 2005; Brocks and Schaeffer, 2008). As this biomarker provides insight into the depositional environment of the source rock, we quantified isorenieratane and other carotenoids using gas chromatography–metastable reaction monitoring mass spectrometry (GC-MRM-MS).

To further extend and complement the previous studies, compound specific isotope analysis (CSIA) using GC-irMS was performed to compare the $\delta^{13}C$ and $\delta^{2}H$ (often referred to as δD) of *n*-alkanes and the isoprenoids pristane (Pr) and phytane (Ph). Hall et al. (2014) reported $\delta^{13}C$ values for isolated *n*-alkanes, but not Pr and Ph, for eight of the 10 asphaltites studied herein. In addition to $\delta^{13}C$ GC-irMS, stable isotopes of hydrogen can be obtained by CSIA. Water is the sole source of hydrogen for photosynthetic organisms and is the main source for most heterotrophic microbes. Hence, hydrogen isotopes carry information about the environmental water from which sedimentary molecules were formed and the subsequent exchange of hydrogen atoms with other molecules (reviewed by Sessions, 2016). The

measurement of the ratio of deuterium to hydrogen ($^{2}H/^{1}H$) in individual compounds is therefore a powerful analytical technique. Of particular interest is the $^{2}H/^{1}H$ values of *n*-alkanes compared to the isoprenoid alkanes Pr and Ph (Dawson et al., 2005; Dawson et al., 2007; Sessions, 2016) which can also assess thermal maturity.

Several potential source units are known within the Cretaceous section in the Otway and Bight basins (reviewed by Hall et al., 2014); however, the majority of these sedimentary rocks contain biomarkers for land-plants, including the angiosperm-specific compound oleanane, which are absent in the fully marine-derived asphaltites. Potential marine source rocks of early Late Cretaceous (late Cenomanian–early Turonian) age have been dredged from the Bight Basin (reviewed by Totterdell and Mitchell, 2009; Hall et al., 2014) which correspond with the oceanic anoxic event at the Cenomanian/Turonian boundary; i.e. OAE 2. However, the absence of isorenieratane in these dredged samples indicates either deposition in a more oxic facies than that which generated the asphaltites or that these rocks are not the source of the asphaltites.

The age of formation of asphaltites is critical for constraining their source and geologic history. In this study, we apply the rhenium-osmium (Re-Os) geochronometer to a subset of 'Family 4' asphaltites. Elevated Re and Os abundances in oil offer the potential for radiometric dating (Georgiev et al., 2016) based on the radioactive β^- decay of ^{187}Re to ^{187}Os with time. There are three critical conditions in order for Re-Os geochronology to succeed: (i) the Os isotopes must be homogenously distributed at the time of oil formation, (ii) the duration of oil generation must be relatively short, and (iii) the Re–Os isotopic system remains undisturbed with time (Georgiev et al., 2016). The method has been successfully applied to dateg oil deposits (e.g. Selby and Creaser, 2005; Finlay et al., 2011; Georgiev et al., 2016). The asphaltene fraction contains the majority of Re and Os in oil (Selby et al., 2007), though resins may also contain measurable Re and Os (DiMarzio et al., 2018); therefore, the asphaltene-rich asphaltites are a suitable target material for Re-Os geochronology. Indeed, recently Re-Os analysis was applied to South Australian asphaltites

(Corrick et al., 2019). This study produced a Re-Os age of 74 ± 26 MA for the complete dataset (n = 16) and 68 ± 15 MA (n = 9) based on a regression of asphaltite data with <2% deviation from the regression of all data points.

All evidence to date based on the analysis of organic molecules points to all of the 'Family 4' asphaltites originating from the same source: a marine shale containing sulphur-rich Type II kerogen, likely associated with a Cretaceous oceanic anoxic event (OAE). If so, the relative abundances of redox-sensitive metals should show strong agreement between samples. We determined metal concentrations thorough quantitative analyses using Inductively Coupled Plasma Mass Spectrometry (ICP-MS). In addition, metals in oils can also provide information on the depositional environment, e.g. conditions favouring sulphate-reducing bacteria (Lewan, 1984) and specific combinations of metals have suggested nutrient-poor/anoxic conditions during sedimentation associated with mass extinction events (Long et al., 2016). Sulphur content in conjunction with organic aromatic biomarkers has also been used to correlate oils with depositional environment (e.g. Hughes et al., 1995).The main aim of this study was to extend our knowledge of the 'Family 4' asphaltites by:

1. Using GCxGC-TOFMS to further characterise the organic molecules present in maltene fractions and to compare this molecular suite with asphaltene hydropyrolysates.
2. Testing the hypothesis that PZE conditions existed during the depositional environment by quantifying isorenieratane and other carotenoid products.
3. Obtaining additional insight into the maturity of the asphaltites by comparing $\delta^{13}C$ and $\delta^{2}H$ of *n*-alkanes and isoprenoids Pr and Ph using CSIA.
4. Testing the hypothesis that the asphaltites are derived from the same source deposited under anoxic conditions based on the quantification of a suite of metals.
5. Constraining the age of the asphaltites using the Re-Os radiometric clock.

The characterization of southern Australian asphaltites by means of the multiple spectroscopic and elemental data types employed in this study could be adapted for use

188 with a wide range of oils, especially asphaltene-rich bitumen samples including both natural
189 seeps and pollution-derived tar balls.

190

191 **2. Materials and Methods**

192 *2.1 Solvents and standards*

193 Solvents were Reagent grade supplied by Honeywell International Inc, (Muskegon, MI,
194 USA). Hydrocarbon authentic standards included NIST SRM2266 (steranes and hopanes)
195 and angiosperm biomarkers, available from a previous study (Eiserbeck et al., 2011).
196 Alkyldiamantane mixture (>98 % purity, also containing adamantanes, triamantanes and
197 tetramantanes) was supplied by PolyDiamond Technologies (Pleasanton, CA).

198

199 *2.2 Asphaltite sample set*

200 Asphaltite samples were obtained from the Primary Industries and Resources South
201 Australia (PIRSA) Core Library. Collection locations and additional data being provided in
202 Table 1 and Fig. 1. Further details regarding collection sites and sample information such as
203 the original sizes and weights are provided in Padley (1995), Edwards et al. (1998) and Hall
204 et al. (2014). Sample 305 was not previously analysed due to uncertainty concerning
205 whether or not the sample was a *bona fide* asphaltite (see Appendix A3.2; Padley, 1995).

206

207 *2.3 Isolation of maltene and asphaltene fractions*

208 The asphaltites were provided in a relatively clean state. It was therefore only necessary to
209 dissolve them in dichloromethane (DCM; ~100 % soluble) and filter through glass wool to
210 remove any small particles of beach debris. The filtrate was then split into two main
211 fractions, maltenes and asphaltenes. The latter was precipitated by adding an excess of
212 chilled pentane and centrifuging for 10 min at 2000 rpm repeatedly until a clear maltene

fraction was obtained. This was reduced in volume by rotary evaporation then taken to dryness under a gentle stream of N_2. The asphaltene content ranged from 46-55% with a mean of 52.1% and relative standard deviation (rsd) of 5.1%, marginally higher than that reported by Hall et al. (2014) of 48.5% (rsd = 7%) for a suite of Family 4 asphaltites. Aliquots of the asphaltene fraction were used for HyPy. The maltene fraction was further fractionated using silica gel chromatography into saturated hydrocarbon (hexane fraction), aromatic hydrocarbon (7:3 hexane: dichloromethane), and polar/resin fractions (1:1 DCM:methanol). To further reduce the complexity of the aromatic hydrocarbon fraction in order to conduct CSIA, aliquots were subject to sub-fractionation using alumina (fully activated) column chromatography based on procedures described by Jiang et al. (2013) to produce subfractions of mainly mono- di, tri and ≥ tetra-cyclic aromatic hydrocarbons and heterocyclic structures.

2.4 HyPy

Asphaltene fractions were redissolved in DCM and activated copper turnings added to remove any associated elemental sulphur. Aliquots of the asphaltene fractions were adsorbed onto pre-combusted silica and rinsed with pentane to remove any residual maltenes. Following method development in which HyPy was conducted both with and without 5 wt.% molybdenum catalyst [$(NH_4)_2MoO_2S_2$], the samples were pyrolysed in the absence of a catalyst using a commercial apparatus (STRATA Technology Ltd) and following standard operating procedures (Grotheer et al., 2015). In brief, the asphaltites were pyrolysed with resistive heating from 25 °C to 250 °C at 300 °C min^{-1}, and then from 250 °C to the final temperature of 550 °C at 8 °C min^{-1} with the final temperature held for 2 min. A constant pressure (150 bar) and flow rate (5 L min^{-1}) of ultra-high purity hydrogen (BOC Group) was maintained throughout the thermal treatment. The released compounds were cold-trapped on a silica-filled trap chilled with dry ice. Products adsorbed on the silica trap were eluted with DCM:MeOH 9:1 by volume. The eluents were reduced in volume and fractionated as described in Section 2.3.

240

241 *2.5 GC-MS*

242 Gas chromatography-mass spectrometry (GC-MS) analyses were performed using a HP-
243 6890A gas chromatograph (Agilent, Santa Clara, CA, USA) interfaced to a HP-5973 mass
244 selective detector (MSD) (Agilent). Analyses of the saturated hydrocarbon fractions were
245 performed using a DB-1ms capillary column and the aromatic fraction using a DB-5ms (both
246 60 m × 0.25 mm internal diameter × 0.25 μm film thickness). The GC oven was programmed
247 from 40 °C (held 1 minute) to 325 °C at 3 °C min^{-1} with a final hold time of 30 minutes. Ultra-
248 high purity helium was used as the carrier gas with a constant flow of 1 mL min^{-1}. Sample
249 injection was 1 μL pulsed splitless at 280 °C, HP-6890 series injector (Agilent). The MSD
250 was operated at 70 eV with a source temperature of 230 °C. Mass spectra were acquired in
251 full scan mode. Peak areas were used to compute molecular ratios. For the saturated
252 hydrocarbon fraction, selected ion monitoring (SIM) mode was also used to analyse the
253 steranes and hopanes. Additional columns and programs were used for the separation of
254 phytane and crocetane (Spaak et al., 2016).

255

256 *2.6 GC×GC-TOFMS*

257 GC×GC-TOFMS was performed using a Leco Pegasus IV GC×GC-TOFMS system (Leco,
258 Saint Joseph, MI, USA). The instrument was equipped with an Agilent 6890 GC and
259 configured with a split/splitless auto-injector (7683B series) and a dual stage cryogenic
260 modulator. Samples were injected in splitless mode. The thermal modulator operates with a
261 dual cold and hot jet. The cold jet gas was dry N_2 chilled with liquid N_2. Column configuration
262 and conditions varied as required to optimise separation of different fractions. Separation in
263 the first dimension was performed using a Rxi 5Sil MS (Restek, Bellefonte, PA, USA) column
264 (60 m × 0.25 mm × 0.25 μm), and the second dimension separation was performed on a DB-
265 17ms (Agilent) column (1.4 m × 0.25 mm × 0.25 μm or 1.4 m × 0.18 mm × 0.18 μm). Helium

266 was used as carrier gas with a constant flow (2 mL min^{-1}). Splitless injection of samples (1 or
267 2 µL) was used with an inlet temperature of 310 °C. The oven was programmed as follows:
268 50 °C (1 min isothermal), then heated at 3.6 °C min^{-1} to 320 °C, where it was held
269 isothermally for 20 min. The modulation period was usually 3–5 s, with a secondary oven
270 and modulator offset of 15 °C. The MS was operated in the positive ion electron ionisation
271 mode at 70 eV with the ion source held at 250 °C. The scan speed was 100 Hz with a range
272 of 45–550 Da. The ChromaTOF (LECO) software package was used for instrument control
273 and data analysis. Peak areas were used to compute molecular ratios. Mass spectra were
274 compared with National Institute of Standards and Technology (NIST, Gaithersburg, MD,
275 USA) libraries plus specialist TOFMS libraries.

276 Both the saturated and aromatic hydrocarbon fractions of the maltenes and asphaltene
277 hydropyrolysates were broadly categorised based on diagnostic fragment ions. Within the
278 saturated hydrocarbon fraction, specific compound groups such as diamondoids were
279 targeted. Specific groups within the aromatic hydrocarbon fraction, such as monoaromatic
280 (m/z 253) and triaromatic steroids (m/z 231), were also targeted. GC×GC-TOFMS peaks
281 containing fragment ions consistent with known compound classes and eluting in the correct
282 time elution window were categorised accordingly (Wang et al., 2006; Booth et al., 2007;
283 Booth et al., 2008; Scarlett et al., 2011). The mass spectra of all peaks with relatively high
284 abundance were manually checked. Full classification was only performed on one
285 representative asphaltite (85) and the others compared for discernible deviations.

286

287 *2.7 Gas chromatography–metastable reaction monitoring mass spectrometry (GC-MRM-MS)*

288 Gas chromatography–metastable reaction monitoring mass spectrometry (GC-MRM-MS)
289 analyses were performed both on combined saturated/aromatic and on a subset aromatic
290 only hydrocarbon fractions. The analyses were performed using a Micromass Autospec
291 Ultima MS interfaced to an Agilent 6890 N GC fitted with an autosampler and a DB-5MS

capillary column (60 m x 0.25 mm × 0.25 µm; J&W Scientific). The GC-oven was programmed from 60 °C (hold 2 min), heated to 150 °C at 10 °C min^{-1}, then heated to 315 °C at 3 °C min^{-1} with a final hold time of 24 minutes. The He gas flow rate was kept constant at 2 mL min^{-1}. The source was operated in electron impact (70 eV) mode at 250 °C, with 8 kV accelerating voltage. Data were acquired and processed using MassLynx 4.0 (Micromass Ltd.) software. Identification of compounds was achieved by comparison with isorenieratane and chlorobactane standards.

2.8 GC-irMS

CSIA was performed using a Thermo Delta V Advantage irMS, coupled to a Thermo Trace GC Ultra via a GC Isolink and Conflo IV. GC conditions were matched to GC-MS (Section 2.4). For carbon isotope analysis, GC column outflow passed through the GC Isolink combustion reactor (copper oxide / nickel oxide, 1000 °C) to combust hydrocarbons to CO_2, while for hydrogen isotope analysis the outflow passed through the high-temperature conversion reactor (graphite-lined, 1420 °C) and was pyrolysed to H_2. The CO_2 and H_2 passed through the Conflo IV interface to the irMS, which measured either *m/z* 44, 45 and 46 for CO_2 or *m/z* 2 and 3 for H_2. The $\delta^{13}C$ and $\delta^{2}H$ values were calculated from the measured masses by Thermo Isodat software. Values were converted to the VPDB / VSMOW scales by comparison with an in-house mixture of *n*-alkane standards (*n*-C_{11}, *n*-C_{13}, *n*-C_{14}, *n*-C_{17}, *n*-C_{18}, *n*-C_{19} and *n*-C_{25}) of known isotopic composition ($\delta^{13}C$ from -25.3 to -32.2 ‰, $\delta^{2}H$ from -104.2 to -268.6 ‰), and commercially-available isotopic standards from Indiana University (http://pages.iu.edu/~aschimme/hc.html): *n*-C_{22} ($\delta^{13}C$ -32.87 ± 0.03 ‰, $\delta^{2}H$ -62.8 ± 1.6 ‰) and squalane ($\delta^{13}C$ -20.49 ± 0.02 ‰ and $\delta^{2}H$ -168.9 ± 1.9 ‰). Samples were measured in triplicate, and standard errors were less than 0.5 ‰ for $\delta^{13}C$ and 5 ‰ for $\delta^{2}H$.

318 *2.9 Rhenium-osmium isotope geochemistry*

319 Five asphaltites, collected at different times from five locations in two different basins, were
320 selected for Re-Os dating (Table 1). Samples were dissolved in DCM and filtered (Section
321 2.3). Weighed asphaltites (0.10−0.25 g) were combined with single ^{185}Re and ^{190}Os spikes in
322 7 mL of concentrated nitric acid. Digestion in quartz vessels in a high-pressure asher
323 achieves complete sample dissolution and equilibration with isotopic tracers. Rhenium and
324 Os were separated using protocols established by the AIRIE Program, and isotopic ratios
325 were subsequently measured using negative thermal ionization mass spectrometry (for
326 methodology, see Georgiev et al., 2016; DiMarzio et al., 2018). Measured Re and Os
327 isotope ratios were corrected for oxygen isotope contributions, mass fractionation, and spike
328 and blank contributions. Two procedural blanks with identical digestion, chemistry, and
329 mass-spectrometry procedures as samples contributed 1.13-1.26 pg Re and 0.03-0.06 pg
330 Os with $^{187}Os/^{188}Os$ between 0.28 and 0.35. These Re and Os blank contributions are low,
331 constituting just 0.1-0.3% and 0.5-0.6%, respectively, of the total Re and Os in each sample
332 analysis. In-house Re (1407 molybdenite, processed through identical chemistry as
333 samples) and Os (N-4) standard solutions measured before sample analyses yielded
334 $^{185}Re/^{187}Re = 0.59661 \pm 0.00005$ (1SD, n = 3) and $^{187}Os/^{188}Os = 0.1235 \pm 0.00014$ (1SD, n =
335 3), which are within the long-term reproducibility of these standards as reported in Markey et
336 al. (2017) and Georgiev et al (2018). The small (~1.3‰) difference between $^{185}Re/^{187}Re$
337 measured in standards and the accepted value for natural Re ($^{185}Re/^{187}Re = 0.59738 \pm$
338 0.00039) was used to correct measured Re isotopic ratios before final data reduction.
339 Uncertainties on Re-Os analyses are calculated by propagation of errors on spike
340 calibrations, weighing, measured ratios, and blank corrections, plus an error magnifier based
341 on the spike-sample ratio. Isochron ages are calculated and plotted using Isoplot v. 4.15
342 (Ludwig, 2003). All Re-Os errors are at the 2-sigma level.
343

344 *2.10 Metal analysis by ICP-MS*

345 Asphaltites were digested in HNO_3 at reflux (~200 °C) then taken to incipient dryness at
346 approximately 200 °C. The residue was then dissolved in HNO_3 and H_2O then suitably
347 diluted for plasma–atomic emission spectroscopy (ICP-AES, Thermo Scientific 6500 iCap
348 Duo) and ICP-MS (7500cs Agilent Technologies) analysis. Metals were measured against
349 AccuTrace High Purity multi-element standards (Choice Analytical, Thornleigh, Australia).

350

351 **3. Results and Discussion**

352 *3.1 Overview characterisation of the maltene and asphaltene hydropyrolysate fractions of*
353 *the asphaltites using GC×GC-TOFMS*

354 The saturated and aromatic hydrocarbon fractions of all ten asphaltites were screened on
355 GC-MS then analysed by GC×GC-TOFMS. The GC-MS analyses of the saturated fractions
356 of the maltenes produced chromatograms with prominent *n*-alkanes but with underlying
357 UCM; the aromatic fractions contained more prominent UCMs (examples of GC-MS TIC for
358 both fractions are shown in Fig. S2). A comparison between samples revealed no major
359 differences that would suggest that any of the samples were not generated from the same
360 source. This reinforced previous studies (reviewed by Hall et al., 2014; Edwards et al., 2016)
361 that found only minor differences consistent with alteration due to weathering. It was not the
362 aim of this study to repeat previous studies although consistency of results was verified.
363 Ratios of biomarkers obtained by GC-MS analyses in the current study were similar to those
364 previously reported (Hall et al., 2014) so the new data reported herein can be confidently
365 appended to previous results. Small differences were sometimes observed between GC-MS
366 and GC×GC-TOFMS data which can be attributed to differences in how masses are
367 quantified by the LECO TOFMS compared to quadrupole MS.

368 Having established that there were no major differences between the maltene fractions of
369 the asphaltites, the asphaltene hydropyrolysates also were compared and very similar
370 GC×GC-TOFMS chromatograms were obtained for all samples. The GC×GC-TOFMS

chromatograms of the asphaltene hydropyrolysates were similar to those of the maltene fractions but also with some clear differences (Fig. S3); most notably, the presence of alkenes in the hydropyrolysates. Using asphaltite 85 as a representative sample, a thorough examination was undertaken of GC×GC-TOFMS chromatographic peaks obtained for the saturated and aromatic fractions of both the maltenes and asphaltene hydropyrolysates (Fig. 2). Peak marker plots (cross plot of retention times in apolar and polar dimensions showing centres of resolved peaks) corresponding to classes shown in Fig. 2 are provided in SI (Figs. S4-5).

With regard to relative peak numbers, i.e. the number of peaks resolved by the ChromaTOF software for each class relative to the total number, of the saturated hydrocarbon fractions, the maltenes and asphaltene hydropyrolysates were very similar (Fig. 2A). However, a large number of the smaller peaks, especially in the hydropyrolysates, could not be readily classified. Peaks representing the majority of the chromatographic area could be categorised although less so for the hydropyrolysates (Fig. 2B). Clearer distinctions could be seen with the bicyclic alkanes more dominant in the hydropyrolysates and tetra/pentacyclic terpanes more abundant in the maltene fraction (Fig. 2B). In the aromatic fractions, peak numbers were similar although monoaromatics (alkylbenzenes, indanes and tetralins) were more prominent in hydropyrolysates (Fig. 2C). As with the saturated fraction, large numbers of minor components could not be classified. Peaks with mass spectra consistent with alkylated naphthalenes represented a greater proportion of the relative chromatographic area in the maltene fraction whereas biphenyls and especially fluorenes were more prevalent in the asphaltene hydropyrolysates (Fig. 2D). Relatively volatile hydrocarbons such as methylnaphthalenes were present in both the maltenes and hydropyrolysates. Because such low molecular weight aromatic compounds are also relatively water soluble it appears that these asphaltites have not experienced substantial water-washing. The higher molecular weight alkylnaphthalenes were less abundant in the hydropyrolysates (Fig. S5 I&J). This trend was even more apparent for the phenanthrenes (Fig. S5 S&T). A substantial proportion

of the mass spectra obtained from the aromatic fractions of both the maltenes and hydropyrolysates were not assigned (Fig. 2D). With the major groupings removed, it could be seen that the unclassified peaks were present throughout the chromatographic elution space (Fig. S5 U&V) but this served to highlight differences between the maltenes and the asphaltene hydropyrolysates. Triaromatic steroids (discussed later in Section 3.2.2) plus some diaromatic tetracyclic structures were particularly prominent. Compounds that were exclusive to the maltene fractions include oxygen and nitrogen-containing heterocyclics although many low abundance compounds were unidentifiable because of weak spectra or confounded by co-elutions even with GC×GC. Higher weight PAHs e.g. fluoranthenes and pyrenes were more abundant in the hydropyrolysates than in the maltene fractions. Taken as a whole, and based on comparison the major identified compound classes of the maltenes and asphaltene hydropyrolysates suggest that the asphaltites have undergone relatively little alteration. However, since comparison of specific biomarkers might show more distinct differences, a more targeted comparison was undertaken.

3.2. Comparison of maltenes and asphaltene hydropyrolysates using selected molecular indicators

3.2.1 Saturated hydrocarbons

An estimate of the thermal maturity of petroleum can be obtained from the odd versus even carbon-numbered *n*-alkanes (Peters et al., 2007). Several indices are widely used for this including the carbon preference index (CPI) and the odd-even predominance (OEP). Values for OEP on the $C_{23–28}$ range of *n*-alkanes present in the asphaltites were found to be just over 1 which is consistent with previous reports (Edwards et al., 1998; Hall et al., 2014). Values significantly below or above 1 suggest low thermal maturity (Peters et al., 2007). Similar OEP values were obtained for *n*-alkanes released by HyPy. Hence, the OEP values for both the maltene and asphaltene hydropyrolysates suggest that the initial crude oil was

thermally mature. However, overprinting of molecular maturity ratios since the time of expulsion from the source may have modified these and other ratios (Curiale et al., 1989).

The most noticeable difference between the asphaltite maltenes and asphaltene hydropyrolysate saturates was the very low abundance or absence of the isoprenoid biomarkers Pr and Ph within the hydropyrolysates. The latter contained a distinct band of alkenes eluting above (i.e. more polar) the alkanes when visualised by GC×GC-TOFMS (Fig. S3). As Ph is known to co-elute with another isoprenoid, crocetane, on commonly used GC capillary columns (Robson and Rowland, 1993) and even using GC×GC, novel methods for both 1D and 2D systems developed by Spaak et al. (2016) were applied to ensure that Pr/Ph ratios in the maltenes were not affected. As crocetane has been used as a proxy for both anaerobic methane oxidation and PZE (reviewed by Spaak et al., 2016), the presence of this biomarker in the asphaltites could affect isotopic signatures. However, none was detected. Further, and due to the low GC×GC-TOFMS peak areas of the isoprenoids in the hydropyrolysates, Pr/Ph ratios could not be calculated with confidence.

Crude oils with prominent *n*-alkanes but also underlying UCMs may result from multiple charges, thus producing mixtures of fresh and biodegraded hydrocarbons (Grice et al., 2000; Bartha et al., 2015). However, Hall et al. (2014) reported no evidence of biomarkers, such as the 25-*nor*hopane series, to indicate substantial biodegradation, and this is consistent with the findings of the present study using GC×GC-TOFMS. Nevertheless, the asphaltites would have spent varying lengths of the time in the ocean as evidenced by the typically small differences in $\delta^{13}C$ and biomarker ratios previously observed in the outer and inner sections of the asphaltites (Hall et al., 2014). Being far more resistant to biodegradation than most hydrocarbons, the cage-like diamondoid hydrocarbonshave proved useful for comparison between oils and with source rocks (e.g. Grice et al., 2000; Wang et al., 2006; Fang et al., 2013). The presence of diamondoids in the ‘Family 4’ samples has not previously been reported, but, using GC×GC-TOFMS analysis, the asphaltites were found to contain relatively low quantities (Fig. 2).

The smallest of the diamondoids, the tricyclic adamantanes, were only detected in trace amounts when the saturated hydrocarbon fraction was not dried. As these lower MW adamantanes are volatile and water soluble, it is likely that they were largely lost during the time the asphaltites spent in the ocean on after stranding (Li et al., 2014). Within the asphaltene matrix, the adamantanes could potentially have greater protection from the effects of evaporation and water washing. Indeed, the asphaltene hydropyrolysates did contain some tricyclic diamondoids but none smaller than dimethyl- or ethyl-substituted adamantanes. However, pentacyclic diamantanes were present, albeit at relatively low concentrations in both the maltenes and asphaltene hydropyrolysates. The sum of chromatographic areas of the methyldiamantanes (ΣMD) relative to pentadecane (*n*-C_{15}) was <0.2 % and <0.1 % for the maltenes and hydropyrolysates respectively. The presence of these structures in all samples permitted the application of the methyldiamantane index (MDI; Fig. S6) which is a commonly applied ratio based on the relative stability of the isomers (Chen et al., 1996). Despite the relatively low abundance of the methyldiamantanes, which can reduce the signal to noise ratio of the instrument and hence increase variability, there was little disparity among the maltene fractions, or between the hydropyrolysates, of the asphaltites (Fig S7A). On average the MDI of the latter of 0.32 (± 0.08 std dev.) was similar to than that of the maltene fraction, 0.38 (± 0.7 std dev.). The relationship between the methyldiamantanes and the parent structure was also similar among asphaltites and between maltenes and hydropyrolysates (Fig. S6B). Overall, there was no significant difference in diamondoid ratios between the maltenes and asphaltene hydropyrolysates that suggests that the thermal maturity of the source rock was low when the original crude oil was generated and that there has been no significant thermal alteration since the asphaltenes were formed.

Steranes and hopanes are two of the most important widely reported classes of biomarkers due to the ubiquitous occurrence of their biogenic precursors, steroids and hopanoids, in living organisms (Peters et al., 2007; Whiteside and Grice, 2016). Steranes and hopanes

were previously identified in many of the asphaltites investigated (Padley, 1995; Edwards et al., 1998; Hall et al., 2014). For the recently analysed asphaltite sample 305, the ratios of specific steranes and hopanes obtained from GC-MS analyses were found to be similar to previously analysed asphaltites. For example, Hall et al. (2014) reported Ts/(Ts + Tm) to be in the range 0.37 – 0.40 for the Family 4 asphaltites; in the present study, sample 305 had a ratio of 0.37. Although the profile of regular steranes in the maltenes was similar to that of the hydropyrolysate, diasteranes were undetectable in the latter (Fig. 3) consistent with previous studies that have reported their absence from hydropyrolysates (Sonibare et al., 2009). There was a relative decrease in C_{27} αββ20R and an increase in C_{27} ααα20R compared to the maltene fraction (Fig. 3). Several commonly applied sterane indices showed very similar mean ratios derived for maltenes and from hydropyrolysates (Fig. S7). Hopane ratios were also generally similar in the maltenes and hydropyrolysates (Fig. S8) with the exception of C_{29}/C_{30} hopanes (C_{29} 17α(H),21β(H)-hopane/C_{30} 17α(H),21β(H)-hopane) which was much larger in the asphaltene hydropyrolysates (Fig. 4). The greater abundance of C_{29} relative to C_{30} hopane has been previously noted for hydropyrolysis products (Sonibare et al., 2009). The absence of 18 α (H) 22,29,30 trisnorhopane (Ts) from the asphaltene hydropyrolysate (Fig. 3 and S9) is normal as it is a rearrangement product (Sonibare et al., 2009). The ratio of the βα to αβ C_{29} hopanes of *ca* 0.13 was found to be the same in both the maltenes and the asphaltene hydropyrolysates; Hall et al (2014) previously reported the same ratio for βα to αβ C_{30} hopanes.

The C_{30} triterpane gammacerane has been used as an indicator of water column stratification (Damste et al., 1995; Grice et al., 1998). Hall et al. (2014) reported the ratio of gammacerane to C_{31}R hopane of 0.17 whereas the current study found this to be *ca* 0.36 and the gammacerane index (gammacerane/(gammacerane + C30 hopane) to be *ca* 0.11 for all asphaltites. Gammacerane was also detected in the asphaltene hydropyrolysates with marginally lower values (gammacerane index *ca* 0.10). The lack of evidence for biodegradation and the near equivalence of the hydropyrolysates and maltene fraction

505 suggest that water column stratification was either weak or intermittent (Peters and
506 Moldowan, 1993).

507 Occuring only in the asphaltene hydropyrolysates were some hopenes, two of which were
508 tentatively assigned based on elution positions and mass spectra reported previously to be
509 present in West African oil seeps (Love et al., 1996; Meredith et al., 2008). Eluting just
510 before Tm, and slightly in the more polar dimension when analysed by GC×GC-TOFMS (Fig.
511 S9), 22,29,30-trisnorhop-17(21)-ene was tentatively identified based on mass spectral
512 comparison (Meredith et al., 2008). Eluting slightly later than Tm (Fig. S9) was a peak
513 consistent with 22,29,30-trisnorhop-16(17)-ene (Meredith et al., 2008; Sonibare et al., 2009).

514

515 *3.2.2 Aromatic compounds*

516 Within the aromatic hydrocarbon fractions, prominent bi and tricyclic hydrocarbons and
517 dibenzothiophenes (DBTs) were observed (Fig. S10). Phenanthrene and its alkylsubstituted
518 isomers have been used for various biomarker indices in the estimation of maturity e.g. the
519 methylphenanthrene ratio (MPR) and the methylphenanthrene index (MPI-1). The latter is
520 used to calculate an eqivalent vitrinite reflectance (Rc) (%). Using GC×GC-TOFMS, the
521 MPR for the asphaltite maltenes (Fig. S11) of 0.73 (± 0.07std dev.) was similar to that of
522 *ca* 0.67 reported by Hall et al. (2014) using GC-MS. The latter also reported MPI-1 values of
523 about 0.64, which are a little higher than that of 0.45 (± 0.03 std dev.) calculated using
524 GC×GC-TOFMS. This infers a slightly lower Rc value of 0.67 % compared to the *ca* 0.77 %
525 calculated based on GC-MS. The previously unanalysed asphaltite sample 305 possessed
526 ratios in agreement with the Family 4 samples. These indices when applied to the
527 asphaltene hydropyrolysates (Fig. S11) produced substantially greater ratios implying a
528 higher Rc of 0.89 %. A similar differential was reported by Reinhardt et al. (2018) between
529 kerogen hydropyrolysates and maltene fractions. A slight opposite trend was observed for
530 the ratios of DBT/MDBT (Fig. S11).

Phenanthrene has also been used in conjunction with DBT either in terms of the ratio of the parent structures (DBT/P) or the methyl-substituted analogues (MDBT/MP). The relationship between DBT/P and Pr/Ph has been used to provide insight into depositional environment (Hughes et al., 1995). However, the crossplot of the DBT/P to Pr/Ph ratios resulted in the asphaltites clustering at the intersection and outside of zones 1b, 2 and 3 (Fig. S12) as defined by Hughes et al. (1995). Although there is some flexibility in the boundaries of these zones, these data are of somewhat limited use in the determination of depositional environment, but highlight the distinctiveness of the asphaltites.

Another important class of aromatic biomarkers are the mono- and triaromatic steranes. Hall et al. (2014) reported the presence of the latter in eight of the asphaltites studied herein. The additional asphaltites analysed in the current study also contained a range of triaromatic steroids with the *m/z* 231 base peak in similar proportions. Using GC×GC-TOFMS, all of the asphaltites were also found to contain a series of methylated triaromatic steranes with base peak *m/z* 245 and $C_{21\text{-}22}$ and $C_{27\text{-}29}$ C-ring monoaromatic steranes with base peak *m/z* 253. The latter structures are reported to be precursors of triaromatic steroids and are present at earlier maturity (Peters et al., 2007). The ratio of monoaromatic (MA) to triaromatic steranes (TA) therefore gives an indication of thermal maturity: with TA/(TA + MA) close to zero indicating immature and approaching 100 % with increasing maturity. This ratio was approximately 40 % in the maltene fraction of the asphaltites. Hydropyrolysates were found to contain a much smaller range of the monoaromatic steroids with lower relative abundance such that most were below the required signal to noise ratio. Therefore the TA/(TA + MA) ratio could not be calculated.

3.3 Quantification of carotenoid products by GC-MRM MS

Peaks with mass spectra and elution positions of diagenetic products of the carotenoid isorenieratene - i.e. isorenieratane and other aryl isoprenoids - were observed in GC×GC-

TOFMS chromatograms of the aromatic fraction of the asphaltite maltenes but isorenieratane was not observed in the hydropyrolysates. Reinhardt et al (2018) observed that, in their study of Lower Jurassic shales, although isorenieratane was present in all the bitumens analysed, it was not present in the corresponding kerogen hydropyrolysates. However, they concluded that destruction of isorenieratane during the HyPy process was unlikely. MRM was used to quantify the carotenoid products in the asphaltite maltene. These analyses confirmed the relatively high concentrations of isorenieratane and chlorobactane, in all of the asphaltite samples, which implies that PZE existed, at least periodically, during the deposition of their source rock. The mean concentrations of isorenieratane and chlorobactane were calculated, based on external calibration standards, to be 8.8 ± 0.8 standard error of mean (SEM) and 1.4 ± 0.1 SEM μg g^{-1} asphaltite respectively, whereas β-carotane was observed but not quantified with reference to standards. This latter compound was derived from other taxa and most probably from cyanobacteria. Schwark and Frimmel (2004) devised the Aryl Isoprenoid Ratio based on the ratio of low molecular weight (C_{13}-$_{17}$) to higher weight (C_{18-22}) 2,3,6-trimethyl aryl isoprenoids plotted against Pr/Ph and demonstrated that it could be used to assess the persistence of PZE. Using GC×GC-TOFMS with extracted ions *m/z* 133 + 134, the asphaltites were found to have a mean Aryl Isoprenoid Ratio of 0.75 (sd = 0.17), so with Pr/Ph of ~1.2 this suggests persistent rather than episodic PZE conditions.

3.4 Comparison of CSIA $\delta^{13}C$ and $\delta^{2}H$ of n-alkanes and isoprenoids

Hall et al. (2014) previously reported $\delta^{13}C$ GC-irMS analyses for *n*-alkanes (isolated by urea adduction) present in eight of the asphaltites studied herein. These have similar $\delta^{13}C$ from -33.3 to -36.9 ‰. We attribute differences between samples to weathering as the asphaltites have similar thermal maturity. In the present study, *n*-alkanes were analysed simultaneously with Pr and Ph so that comparisons could be made. The $\delta^{13}C$ values for the *n*-alkanes were a little heavier (*n*-C_{17}– *n*-C_{18}: -31.3 to -32.0) than reported by Hall et al. (2014), likely a consequence of analysis within a mixture, with little variation between asphaltites (Fig. 5).

585 Asphaltite sample 305 showed $\delta^{13}C$ values similar to the 'Family 4' asphaltites. Although
586 mean $\delta^{13}C$ values of Pr and Ph were depleted relative to *n*-C_{17} and *n*-C_{18} suggesting an
587 "inversion" from the normal pattern (sensu Tang et al., 2017) observed rarely in Phanerozoic
588 deposits including Upper Cretaceous (Hayes et al., 1990), the isoprenoid alkane carbon
589 isotope ratios were not significantly different to their *n*-alkane counterparts (Fig. 5). Although
590 interferences by co-eluting compounds within the UCM cannot be ruled out, analysis by
591 GC×GC-TOFMS showed that co-eluting compounds with greater polarity represented <1%
592 of the peak areas of either Pr or Ph. Due to the very low abundances of Pr and Ph in
593 hydropyrolysates, $\delta^{13}C$ values could not be obtained for these but *n*-alkanes had values (for
594 carbon) similar to those found in the maltene fraction (Fig. S13).

595 In addition to ^{13}C isotopes, CSIA of stable isotopes of hydrogen, especially the comparison
596 of *n*-alkanes and isoprenoids, is useful for determining their relative maturity (Dawson et al.,
597 2005; Dawson et al., 2007; Sessions, 2016). Such $\delta^{2}H$ measurements were conducted on a
598 subset of the asphaltite aliphatic fractions. All showed similar profiles with $\delta^{2}H$ values for *n*-
599 alkanes of *ca* -100 to -120 ‰. These values were marginally less negative, i.e. more
600 enriched, than values previously reported (*ca* -105 to -130 ‰) for relevant asphaltites
601 (Boreham, 2008). The offset between the isoprenoid biomarkers, Pr and Ph, and *n*-alkanes
602 of *ca* -60 ‰ (Fig. 6) was different to the near equivalence in values that is associated with a
603 mature oil, e.g. the two Perth Basin crude oils reported by Dawson et al. (2005). Assuming a
604 similar H-catagenic pathway for both Permo-Triassic sourced Perth Basin oils and the
605 Cretaceous sourced asphaltites, the latter has a lower thermal maturity. Although it has been
606 reported that biodegradation enriches *n*-alkanes, especially those <C_{23} (Asif et al., 2011),
607 this is highly unlikely to explain all of the observed offset especially as there is no evidence
608 of extensive biodegradation within this set of asphaltites (Hall et al., 2014). In the Pre-oil to
609 Post-oil continuum classification system proposed by Curiale (1986), the $\delta^{2}H$ values (Fig. 6)
610 suggest that the origin of the initially discharged asphaltic bitumen was closer to pre-oil with
611 limited migration from the source rock. This is somewhat at odds with other characteristics.

612 For example the Rc values for the asphaltites, including the asphaltene hydropyrolysates,
613 implied that their source rocks were within the oil window (section 3.2.2) at the time of
614 generation/expulsion. Factors that may affect $\delta^{2}H$ values were reviewed by Sessions (2016).
615 The H-isotope offset between coexisting isoprenoids and *n*-alkanes is one approach (e.g.
616 Dawson et al., 2005; Dawson et al., 2007; Maslen et al., 2012), but is yet to be quantified as
617 a formal parameter suitable for use in models of hydrocarbon evolution and may be
618 influenced by kinetic fractionations.

619

620 *3.5 CSIA of $\delta^{13}C$ aromatic compounds*

621 Obtaining $\delta^{13}C_{arom}$ for individual aromatic compounds is potentially of diagnostic value, such
622 as in establishing facies type (Maslen et al., 2011) but is challenging due to the complexity of
623 aromatic fractions of the asphaltites. Preliminary investigations of the whole aromatic
624 fractions from both the maltene fractions and the asphaltene hydropyrolysates showed that
625 for $\delta^{13}C_{arom}$, co-elution was such that little discriminatory information was revealed.
626 Consequently, additional subfractionation was performed using alumina-based
627 chromatography. The target compounds for $\delta^{13}C_{arom}$ were bi- and tricyclic aromatic
628 hydrocarbons. Analyses by GC×GC-TOFMS had revealed that the majority of the interfering
629 compounds were monoaromatic hydrocarbons such as alkylated benzenes, indanes, and
630 tetralins. With these removed by the subfractionation of the aromatic fraction, several of the
631 dominant bi-and tricyclic aromatics were sufficiently resolved to obtain $\delta^{13}C_{arom}$ values on
632 apparently single resolved peaks. Similarly, the further removal of the bicyclic aromatics
633 reduced the interference for the lower molecular weight tricyclic aromatic hydrocarbons such
634 as phenanthrene and methylphenanthrenes plus the heterocyclic dibenzothiophenes. It
635 should be noted that in such a complex mixture, co-elution can still occur leading to
636 interferences with $\delta^{13}C_{arom}$ values. These values may also be affected by incomplete
637 recovery of compounds within a single fraction.

A small depletion was observed in mean $\delta^{13}C_{arom}$ values in the asphaltene hydropyrolysates compared to the asphaltite maltenes for the triaromatic hydrocarbon phenanthrene (P) but this was less prominent for the dimethylphenanthrenes (DMP); the heterocyclic dibenzothiophene (DBT) possessed the same values, *ca* -30 ‰ for both. Combining the ratio of DBT/P (and that of Pr/Ph) with $\delta^{13}C$ of dimethylphenanthrenes in a cross-plot has been shown to reveal information about marine versus terrigenous input (Maslen et al., 2011). Lower ratios combined with increasingly negative $\delta^{13}C_{arom}$ was correlated with more marine-dominated input whereas higher ratios coupled with greater enrichment was associated with terrigenous input (Maslen et al., 2011). Applying the same approach to the asphaltites (Fig. S14) strongly suggested a marine-dominated input consistent with previous studies (reviewed by Hall et al., 2014; Edwards et al., 2016). A cross-plot for the asphaltene hydropyrolysates Pr/Ph and $\delta^{13}C_{arom}$ DMP was not possible due to the virtual lack of pristane and phytane in the latter.

3.6 Quantification of elements other than carbon

Elements were quantified using a digest method on whole asphaltites with analysis by ICP-MS. Many of the metals were in very low abundance (Table S1) with many <0.1 ppm. However, some metals were present in much higher concentrations (Table 2). Sulphur was the most abundant element with similar values for all asphaltites in the range 30400 – 34700 µg g^{-1}. This similarity in concentrations was apparent for most of the elements measured in all samples (Tables 2 and S1). However, for some metals, most notably calcium (Ca), aluminium (Al), magnesium (Mg), sodium (Na) and iron (Fe), there was considerable variation. Although there was no obvious pattern to the concentration variation, the asphaltite CL1, collected in 2005 from the Eyre Peninsula, i.e. the most westerly sample (Table 1, Fig. 1, tended to have consistently elevated concentrations for some of the metals (Table 2). Asphaltite MH1, also collected in 2005 from the western side of the Eyre

664 Peninsula, possessed an atypically high concentration of boron (B = 73.3 µg g^{-1}) and also
665 had the highest abundance of Na (Table 2).

666 Of particular interest are the values for nickel (Ni) and vanadium (V) with the Ni/V index
667 being low; *ca* 0.1 for all samples (Table 2). Lewan (1984) attributed high V/(V + Ni) in
668 conjunction with high sulphur content as indicating conditions favouring sulphate-reducing
669 bacteria. Our analyses fitted this category with median V/(V + Ni) of 0.92 and S of 3.2 %.
670 The asphaltites exhibit very low Selenium concentrations in conjunction with high V. This
671 combination has previously been attributed to low nutrient/anoxic conditions during
672 sedimentation and associated with mass extinction events (Long et al., 2016) although no
673 Se data across the Cretaceous–Paleogene boundary was available for the latter study.
674 Taken together, these results indicate highly anoxic conditions in a marine environment with
675 a low nutrient supply (Lewan, 1984; Long et al., 2016).

676 The data obtained from the metals analysis can also be used in conjunction with organic
677 biomarkers. For example, Hughes et al. (1995) reported that a plot of sulphur content versus
678 the dibenzothiophene/phenanthrene (DBT/P) ratio can be used to correlate oils with
679 depositional environment. Oils with high DBT/P do not necessarily have high sulphur and,
680 conversely, high sulphur is not always associated with high DBT/P (Hughes et al., 1995).
681 The asphaltites have a relatively high sulphur content (*ca* 3.2 %) compared to the DBT/P
682 ratio of close to unity (Fig. S13).

683 *3.7 Rhenium-osmium geochronometry*

684 Five analysed asphaltites from five sampling locations in two basins have remarkably similar
685 Re (3.9-4.2 ppb) and Os (0.043-0.045 ppb) contents (Table 3). These concentrations are
686 relatively low for asphaltene-rich samples, but fall within the range of Re-Os contents for
687 petroleum products (see Georgiev et al., 2016). The remarkably uniform Re and Os contents
688 in these five samples provide strong evidence for a common origin, in agreement with
689 organic geochemical data (Hall et al., 2014 and further geochemical data from current

study). A common origin for the five asphaltites is strongly supported by their similar $^{187}Re/^{188}Os$ isotopic ratios (Fig. 7; Table 3). Importantly, most of the Re and Os in oils is typically hosted in the asphaltene fraction (Georgiev et al., 2016) though resins may also contain Re and Os (DiMarzio et al., 2018). As such, reported Re-Os contents and isotopic ratios for the analysed samples indicate a common origin specifically for the asphaltene fractions in the five asphaltites which have relatively high asphaltene contents (*ca*50 %). This is a valuable observation because asphaltene fractions are typically less accessible for traditional organic geochemical studies than the lighter maltene fractions of oils, which may or may not (in the case of mixed oil) share a common source and age with the asphaltenes. In addition, the Re-Os isotopic integrity of asphaltene-rich materials (e.g., this study) is likely to be preserved because, compared to maltenes, asphaltenes are generally more resistant to secondary alteration from evaporation or biodegradation on transport.

On a Re-Os isochron diagram, our asphaltites define a linear array yielding a Model 1 age of 103 ± 22 Ma and an initial $^{187}Os/^{188}Os$ = 0.44 ± 0.18 (n = 5) (Fig. 7). The relatively large uncertainty in this regression, despite the robust analytical precision of individual data points and the excellent fit of the data points along the isochron (MSWD = 1.2), is attributed to the limited spread in Re-Os isotopic ratios. That is, the stability of a regression line through closely spaced points is less than if the same points are spread out in x-y space. This statistic presents a larger age uncertainty.. Our 103 (± 22 Ma) Ma Re-Os age differs somewhat from an isochron age of 68 ± 15 Ma (*n* = 9, Model 1) for a subset of asphaltites recently reported by Corrick et al. (2019), although the 95 % confidence intervals marginally overlap between studies. A 16-point regression for all Re-Os data reported by Corrick et al. (2019) gave a slightly older age with larger confidence intervals (74 ± 26 Ma, Model 3) which is in greater accord with the current study. In fact, six out of the seven points excluded to produce the Model 1 age in the latter study, overlap with the Model 1 age of 103 ± 22 Ma defined by our five precise data points (Fig. 6), suggesting that their discarded points may have real geologic significance, whereas their retained data points defining the 68 ± 15 Ma

may represent geological and/or analytical outliers. The analytical uncertainties for data reported by Corrick et al. (2019) are much larger than the analytical errors reported herein. Reporting larger analytical errors has the effect of more readily achieving Model 1 ages and thus, better MSWD values for isochrons. This large-error advantage can give an unjustified sense of accuracy by simply improving isochron statistics. In an attempt to consolidate the Re-Os data derived from Corrick et al. (2019) and the current study, we have plotted all the data on the same isochron plot (Fig. 6). This highlights the analytical errors and demonstrates how closely some of asphaltite data overlaps between studies.

Our 103 Ma Re-Os age suggests that asphaltites were generated in the Cretaceous (late Albian), noting that incorporation of full analytical uncertainty (± 22 Ma) permits an Aptian-early Campanian timing for oil generation (125-81 Ma). This timing is the most likely when taking into account all available data (including all data reported by Corrick et al., 2019; see Fig. 6). Recent studies identify several Cretaceous marine shales as potential source rocks for the 'Family 4' asphaltites (e.g. Padley, 1995; Edwards et al., 1998; Boreham et al., 2001; Totterdell et al., 2008; Hall et al., 2014; Edwards et al., 2016). In a comparative and comprehensive geochemical study of asphaltites with on-shore source rock analogs, Boreham et al. (2001) concluded that the asphaltite source rock was mid-Cretaceous (middle to late Albian), in excellent agreement with our asphaltite Re-Os age of 103 Ma. Particularly diagnostic is the presence of high V/Ni metalloporphyrins in the asphaltites matching the metalloporphyrins in the Albian Toolebuc Formation, and the similar sulphur contents of both (Boreham et al., 2001). The generally immature Toolebuc formation typically possesses high organic carbon values (up to 20 %), and stable atomic H/C ratios (*ca*1.1) but variable atomic O/C ratios and highly variable sulfur content (see Boreham and Powell, (1987) for in-depth description of Toolebuc formation organic matter). While details differ, the specific organic geochemistry of the asphaltites suggests a marine source rock likely deposited during one of the Cretaceous oceanic anoxic events (OAE; c.f., Jenkyns, 2010).

744 The initial $^{187}Os/^{188}Os$ ratio of petroleum is thought to reflect the $^{187}Os/^{188}Os$ in the source
745 rock at the time of oil generation. Therefore, the initial $^{187}Os/^{188}Os$ of the studied asphaltites
746 provides some important constraints on the age of their potential source rock and possibly
747 also the timing of generation and expulsion. Ideally, Re-Os isotopic studies on both
748 petroleum and potential source rocks should be used together for oil-source rock
749 correlations. In the absence of Re-Os data on potential source rocks in the area, we draw
750 from published Os isotopic constraints from time equivalent Cretaceous shales elsewhere.
751 Worldwide, marine sediments deposited during the early Aptian OAE1a (~120 Ma) and the
752 Cenomanian-Turonian OAE2 (~93.5 Ma) show remarkably similar stratigraphic patterns of
753 initial $^{187}Os/^{188}Os$ ratios (Turgeon and Creaser, 2008; Tejada et al., 2009; Bottini et al., 2012;
754 Du Vivier et al., 2015). Both OAE events are characterized by a pre-OAE baseline of
755 relatively stable and high values (~0.4-0.9 for sections globally), a sharp decline to values of
756 ~0.15-0.20 during most of the OAE event, and a sharp recovery to pre-OAE values of ~0.4-
757 0.9 in most sections (values remain low at ~0.20 in post-OAE1a sedimentary rocks studied
758 by Bottini et al., 2012). This uniform pattern of Os isotopic changes detected over a wide
759 geographic range suggests that similar Os isotopic ratios may be typical for OAE1a and
760 OAE2 strata from South Australia as well. To our knowledge, there are no published Re-Os
761 data on OAE1b (early Albian, ~110 Ma) sections.

762 Assuming that potential marine source rocks from South Australia had similar Os isotopic
763 ratios to their time equivalents elsewhere, the Re-Os isochron age and initial Os isotopic
764 constraints can discriminate between Cenomanian-Turonian (OAE2) and lower Aptian
765 and/or lower Albian (OAE 1a, OAE 1b) shales as potential source rocks for South Australian
766 asphaltites. *First*, petroleum generation must postdate source rocks deposition. Further,
767 significant overburden of source rocks is generally required to elevate temperatures to levels
768 required for kerogen breakdown. In this respect, our age of 103 ± 22 Ma favours OAE1a
769 sediments (~125 Ma) as the source rock for the asphaltites. Sediments deposited during
770 OAE2 (~94 Ma) are deposited close to the lower limit of our age uncertainty, but are

permissible with the Re-Os Model 1 age suggested by Corrick et al. (2019), and the time needed to acquire sufficient sedimentary overburden to reach the oil window decreases the likelihood that OAE2 sediments were the asphaltite source rocks. Although sediments deposited during the OAE1b (~110 Ma) are potentially the source of asphaltites, this scenario would require fast accumulation rates to create sufficient overburden for petroleum generation.

Second, the source rock must have the needed time for in-growth of radiogenic ^{187}Os to permit the isochron initial $^{187}Os/^{188}Os$ of 0.44 ± 0.18, as determined by the asphaltite regression. Because data from the literature show that shales from both the OAE1a and OAE2 have relatively low $^{187}Re/^{188}Os$ isotopic ratios, typically lower than 300 and often lower than 100 (Turgeon and Creaser, 2008; Tejada et al., 2009; Bottini et al., 2012; Du Vivier et al., 2015), the radiogenic growth of ^{187}Os with time in these shales is limited. Therefore, younger intervals (OAE2 and OAE1b) with initially low $^{187}Os/^{188}Os$ ratios of ~0.2 are a less plausible source. For example, we calculate that at 81 Ma (our youngest possible age), OAE2 intervals starting with an $^{187}Os/^{188}Os$ initial of 0.200 (e.g., data from Turgeon and Creaser, 2008) would have a maximum $^{187}Os/^{188}Os$ of 0.237, which is lower than the isochron-derived $^{187}Os/^{188}Os$ for the asphaltite samples. Intervals from OAE1a (data from Tejada et al., 2009), however, are older (125 Ma) and provide a longer time interval for in-growth of radiogenic ^{187}Os. Accordingly, the $^{187}Os/^{188}Os$ is significantly higher (0.307 at 103 Ma and 0.348 at 81 Ma); these $^{187}Os/^{188}Os$ ratios overlap the 0.44 ± 0.18 analytical uncertainty in our Os initial ratio. Hence, OAE1a sediments could potentially produce the $^{187}Os/^{188}Os$ signature of asphaltites at the extreme lower end allowed by our uncertainties. Most sediments deposited immediately before or after the OAE1a and OAE2 events have higher initial $^{187}Os/^{188}Os$ than those within the OAE intervals (with initial $^{187}Os/^{188}Os$ ratios ~0.15-0.20), and therefore represent a more plausible source for our asphaltites. Specifically, most pre- and post-OAE2 sediments have a typical range of initial $^{187}Os/^{188}Os$ between 0.6 and 0.9 (Turgeon and Creaser, 2008; Du Vivier et al., 2015). These values are

higher than the permissible range of initial $^{187}Os/^{188}Os$ from our asphaltite regression (0.44 ± 0.18) and hence argue against a genetic link between OAE2-related sediments and the asphaltites. In contrast, most pre- and some post-OAE1a sediments have a typical range of initial $^{187}Os/^{188}Os$ between 0.35 and 0.65 (Tejada et al., 2009; Bottini et al., 2012), which change little with time because of low $^{187}Re/^{188}Os$ ratios in the sediments, and therefore are a plausible source for the asphaltites. The Re-Os isochron age of 103 Ma is in good agreement with a proposed off-shore middle to late Albian source rock and potentially equivalent to the present-day on-shore Toolebuc Formation (Boreham et al., 2001). Note, however, that Os isotopic constraints are not available for OAE1b (~110 Ma) sediments. Though imprecise, this 103 ± 22 Ma age might also be interpreted as the first indirect Re-Os dating of the OAE1b, provided OAE1b sediments were buried rapidly, reached the oil window, and generated asphaltites shortly after the OAE1b event.

4. Summary and Conclusions

A comprehensive comparison of the peaks resolved by GC×GC-TOFMS in maltenes and asphaltene hydropyrolysates of asphaltite samples collected along the coast of southern Australia showed considerable similarity (Fig 1). Many of the differences can be explained by the presence of alkenes in the hydropyrolysates, normal for this process, which added to the complexity of the chromatograms (Fig. S4 and S10). Further differences were due to the absence of rearranged triterpenes (e.g. Ts, C_{29}Ts and diasteranes) in the hydropyrolysates (Fig. 4). Commonly applied biomarker and indicator ratios were generally similar for both the maltene and hydropyrolysates phases (Fig. S7-S9). In addition, individual compounds within the maltenes were isotopically similar to those in the asphaltene hydropyrolysates. These observations, together with the lack of specific indicators of biodegradation, suggest that there has been relatively little alteration to the organic chemical composition of these ‘Family 4’ asphaltites since their formation, although samples of the original asphaltic bitumen would be required in order to confirm this (see Hall et al., 2014 for discussion on possible origins of

initially discharged asphaltic bitumen). Following discharge, solid bitumens may act as natural preservatives which protect the hydrocarbons within the asphaltites from biodegradation after the bitumen surface solidified into their glassy black appearance (Song et al., 2015). This lack of further substantial chemical alteration is supported by the co-linearity of asphaltite samples in Re-Os isochron.

This study supports previous biomarker evidence (reviewed by Hall et al., 2014; Edwards et al., 2016) which points towards a marine depositional environment. There is clear evidence for anoxic and indeed PZE conditions from the presence of chlorobactane and isorenieratane in relatively high abundance and the Aryl Isoprenoid Ratios coupled with Pr/Ph suggested the PZE conditions were persistent. Metal concentrations are also consistent with anoxic conditions (Table 2 and Table. S1). The relative abundance of gammacerane, an indicator of water stratification (Damste et al., 1995; Grice et al., 1998), was however moderately low in the asphaltites. Other biomarkers that have been associated with PZE such as crocetane were absent.

The Re-Os age from this study suggests a Cretaceous (103 ± 22 Ma) generation age for South Australia asphaltites. This age range is consistent with the Re-Os age of 74 ± 26 Ma reported previously (Corrick et al., 2019) for a larger dataset (n = 16). From the Cretaceous OAE sediments put forward as possible sources for the asphaltites, this age highly favours the older, OAE1a (~125 Ma) sediments over the younger, OAE2 (~94 Ma) sediments for their source rock. Initial $^{187}Os/^{188}Os$ constraints from asphaltites, compared with OAE2 and OAE1a sediments worldwide (assuming the Cretaceous section off-shore South Australia is similar to other global sections) also suggest that OAE1a sediments provide the more plausible source rock. Our 103 Ma Re-Os age is also in good agreement with an off-shore middle to late Albian source rock (equivalent to the Toolebuc Formation). If OAE1b sediments were buried sufficiently rapidly, and generated asphaltic bitumen shortly after the OAE1b event, this albeit imprecise 103 ± 22 Ma age might also be interpreted as the first

indirect Re-Os dating of the OAE1b. We reiterate that Re-Os studies to directly date potential source rocks from South Australia are needed to underpin these interpretations.

A comparison of δ^2H of *n*-alkanes and isoprenoids Pr and Ph using CSIA revealed a considerable offset suggesting that the asphaltite was generated at lower thermal maturity than that implied by other conventional biomarker maturity indicators. Unless kinetic fractionations influenced the measurement (Sessions, 2016), the large pristane/*n*-alkane δ^2H offset suggests that the origin of the initially discharged asphaltic bitumen was closer to pre-oil. Such low thermal maturity requires relatively low overburden that may be achieved in the short time span between OAE1a (or even shorter time for OAE1b) source rock deposition and asphaltic bitumen generation at Re-Os age of 103 ± 22 Ma. Under such circumstances migration from the source rock would be highly limited.

This multi spectroscopic and elemental study of southern Australian asphaltites has revealed new insights into their origin and character with a constrained generation age of 103 ± 22 Ma. Carotenoid derivatives indicative of persistent, strong PZE depositional environment supports a likely Cretaceous OAE1a (~125 Ma) source rock although OAE1b cannot be ruled out. Biomarker maturity indicators are generally consistent with low thermal maturity, characteristic of an early oil window. However, the pristane/*n*-alkane δ^2H offset suggests an even lower maturity for the asphaltic bitumen associated with the Family 4 asphaltites which would limit migration from the source rock. The range of methods applied in this study could be adopted for use with asphaltene-rich samples including both naturally-derived and pollution-derived petroleum products.

Author Contributions

KG designed the project. *GC-irMS* isotopic analyses was performed by AH. Re-Os was analysed and data interpreted by SG and HS. MRM was conducted by RS. All other

chemistry and analyses was performed by AS. AS wrote the manuscript, HS and SV contributed the Re-Os sections, and input was received from all co-authors.

Acknowledgements

We thank Dianne Edwards (Geoscience Australia), David McKirdy and Tony Hall (Organic Geochemistry in Basin Analysis Group, University of Adelaide) for donating the asphaltite samples from their archival collections housed in the PIRSA Core Library. Dianne Edwards also provided valuable feedback on an early draft of this manuscript. The manuscript was further improved thanks to the reviews provided by Will Meredith, Chris Boreham and Joseph Curiale. We thank Robert K Nelson of Woods Hole Institute, USA for supplying TOF mass spectral library and for supply of authentic standards of steranes and hopanes. We also thank Hendrik Grotheer for assistance with HyPy, and Peter Hopper and Geoff Chidlow for assistance with GC-MS.

Funding

This work was supported by Chevron Australia Pty Ltd Project No. RES-55182. For the Re-Os analytical work, the CHRONOS project supported by Eni Norge, Lundin and Aker BP shared in salary support for authors HS and SG.

References

Arey, J.S., Nelson, R.K., Reddy, C.M., 2007. Disentangling oil weathering using GCxGC. 1. Chromatogram analysis. Environmental Science & Technology 41, 5738-5746.

Asif, M., Fazeelat, T., Grice, K., 2011. Petroleum geochemistry of the Potwar Basin, Pakistan: 1. Oil-oil correlation using biomarkers, delta C-13 and delta D. Organic Geochemistry 42, 1226-1240.

Bartha, A., De Nicolais, N., Sharma, V., Roy, S.K., Srivastava, R., Pomerantz, A.E., Sanclemente, M., Perez, W., Nelson, R.K., Reddy, C.M., Gros, J., Arey, J.S., Lelijveld, J., Dubey, S., Tortella, D., Hantschel, T., Peters, K.E., Mullins, O.C., 2015. Combined Petroleum System Modeling and Comprehensive Two-Dimensional Gas Chromatography To Improve Understanding of the Crude Oil Chemistry in the Llanos Basin, Colombia. Energy & Fuels 29, 4755-4767.

Bishop, A.N., Love, G.D., McAulay, A.D., Snape, C.E., Farrimond, P., 1998. Release of kerogen-bound hopanoids by hydropyrolysis. Organic Geochemistry 29, 989-1001.

Booth, A.M., Scarlett, A.G., Lewis, C.A., Belt, S.T., Rowland, S.J., 2008. Unresolved Complex Mixtures (UCMs) of Aromatic Hydrocarbons: Branched Alkyl Indanes and Branched Alkyl Tetralins are present in UCMs and accumulated by and toxic to, the mussel Mytilus edulis. Environmental Science & Technology 42, 8122-8126.

Booth, A.M., Sutton, P.A., Lewis, C.A., Lewis, A.C., Scarlett, A., Chau, W., Widdows, J., Rowland, S.J., 2007. Unresolved complex mixtures of aromatic hydrocarbons: Thousands of overlooked persistent, bioaccumulative, and toxic contaminants in mussels. Environmental Science & Technology 41, 457-464.

Boreham, C., Krassay, A., Totterdell, J., 2001. Geochemical comparisons between asphaltites on the southern Australian margin and Cretaceous source rock analogues. In: Hill, K.C. and Bernecker, T. (Eds), Eastern Australasian Basins Symposium: a refocused energy perspective for the future. Petroleum Exploration Society of Australia, Special Publication, 531–541.

Boreham, C.J., 2008. Bight Basin marine potential source rocks: a local expression of the Late Cretaceous oceanic anoxic event (OAE) 2? Australian Organic Geochemistry Conference (15th : 2008 : Adelaide, S.A.).

Bottini, C., Cohen, A.S., Erba, E., Jenkyns, H.C., Coe, A.L., 2012. Osmium-isotope evidence for volcanism, weathering, and ocean mixing during the early Aptian OAE 1a. Geology 40, 583-586.

Brocks, J.J., Love, G.D., Snape, C.E., Logan, G.A., Summons, R.E., Buick, R., 2003. Release of bound aromatic hydrocarbons from late Archean and Mesoproterozoic kerogens via hydropyrolysis. Geochim. Cosmochim. Acta 67, 1521-1530.

Brocks, J.J., Schaeffer, P., 2008. Okenane, a biomarker for purple sulfur bacteria (Chromatiaceae), and other new carotenoid derivatives from the 1640 Ma Barney Creek Formation. Geochim. Cosmochim. Acta 72, 1396-1414.

Brocks, J.J., Summons, R.E., 2004. Sedimentary hydrocarbons, biomarkers for early life. In Treatise on Geochemistry, vol. 8 (ed. W. H. Schlesinger), pp. 63–115. Biogeochemistry. Elsevier—Pergamon, Oxford.

Chen, J.H., Fu, J.M., Sheng, G.Y., Liu, D.H., Zhang, J.J., 1996. Diamondoid hydrocarbon ratios: Novel maturity indices for highly mature crude oils. Organic Geochemistry 25, 179-190.

Corrick, A.J., Selby, D., McKirdy, D.M., Hall, P.A., Gong, S., Trefry, C., Ross, A.S., 2019. Remotely constraining the temporal evolution of offshore oil systems. Sci Rep 9, 1327.

Curiale, J.A., 1986. Origin of solid bitumens, with emphasis on biological marker results. Organic Geochemistry 10, 559-580.

Curiale, J.A., Larter, S.R., Sweeney, R.E., Bromley, B.W., Year., pp. 53-72.

Damste, J.S.S., Kenig, F., Koopmans, M.P., Koster, J., Schouten, S., Hayes, J.M., Deleeuw, J.W., 1995. Evidence for gammacerane as an indicator of water column stratification. Geochim. Cosmochim. Acta 59, 1895-1900.

Dawson, D., Grice, K., Alexander, R., 2005. Effect of maturation on the indigenous delta D signatures of individual hydrocarbons in sediments and crude oils from the Perth Basin (Western Australia). Organic Geochemistry 36, 95-104.

947 Dawson, D., Grice, K., Alexander, R., Edwards, D., 2007. The effect of source and maturity on the
948 stable isotopic compositions of individual hydrocarbons in sediments and crude oils from the Vulcan
949 Sub-basin, Timor Sea, Northern Australia. Organic Geochemistry 38, 1015-1038.
950 DiMarzio, J.M., Georgiev, S.V., Stein, H.J., Hannah, J.L., 2018. Residency of rhenium and osmium in a
951 heavy crude oil. Geochim. Cosmochim. Acta 220, 180-200.
952 Du Vivier, A.D.C., Selby, D., Condon, D.J., Takashima, R., Nishi, H., 2015. Pacific Os-187/Os-188
953 isotope chemistry and U-Pb geochronology: Synchroneity of global Os isotope change across OAE 2.
954 Earth and Planetary Science Letters 428, 204-216.
955 Edwards, D.S., McKirdy, D.M., Summons, R.E., 1998. Enigmatic asphaltites from the southern
956 Australian margin: Molecular and isotopic composition. Petroleum Exploration Society of Australia
957 (PESA) 26, 106–129.
958 Edwards, D.S., Vinall, D.R., Corrick, A.J., McKirdy, D.M., 2016. Natural bitumen stranding on the
959 ocean beaches of Southern Australia: a historical and geospatial review. Trans. R. Soc. S. Aust. 140,
960 152-185.
961 Eiserbeck, C., Nelson, R.K., Grice, K., Curiale, J., Reddy, C.M., 2012. Comparison of GC-MS, GC-MRM-
962 MS, and GC x GC to characterise higher plant biomarkers in Tertiary oils and rock extracts. Geochim.
963 Cosmochim. Acta 87, 299-322.
964 Fang, C.C., Xiong, Y.Q., Li, Y., Chen, Y., Liu, J.Z., Zhang, H.Z., Adedosu, T.A., Peng, P.A., 2013. The
965 origin and evolution of adamantanes and diamantanes in petroleum. Geochim. Cosmochim. Acta
966 120, 109-120.
967 Finlay, A.J., Selby, D., Osborne, M.J., 2011. Re-Os geochronology and fingerprinting of United
968 Kingdom Atlantic margin oil: Temporal implications for regional petroleum systems. Geology 39, 475.
969 Frysinger, G.S., Gaines, R.B., Xu, L., Reddy, C.M., 2003. Resolving the unresolved complex mixture in
970 petroleum- contaminated sediments. Environ. Sci. Technol. 37, 1653-1662.
971 Georgiev, S.V., Stein, H.J., Hannah, J.L., Galimberti, R., Nali, M., Yang, G., Zimmerman, A., 2016. Re-
972 Os dating of maltenes and asphaltenes within single samples of crude oil. Geochim. Cosmochim.
973 Acta 179, 53-75.
974 Georgiev, S.V., Zimmerman, A., Yang, G., Goswami, V., Hurtig, N.C., Hannah, J.L., Stein, H.J., 2018.
975 Comparison of chemical procedures for Re-isotopic measurements by N-TIMS. Chemical Geology
976 483, 151-161.
977 Grice, K., Alexander, R., Kagi, R.I., 2000. Diamondoid hydrocarbon ratios as indicators of
978 biodegradation in Australian crude oils. Organic Geochemistry 31, 67-73.
979 Grice, K., Cao, C.Q., Love, G.D., Bottcher, M.E., Twitchett, R.J., Grosjean, E., Summons, R.E., Turgeon,
980 S.C., Dunning, W., Jin, Y.G., 2005. Photic zone euxinia during the Permian-Triassic superanoxic event.
981 Science 307, 706-709.
982 Grice, K., Schaeffer, P., Schwark, L., Maxwell, J.R., 1996. Molecular indicators of
983 palaeoenvironmental conditions in an immature Permian shale (Kupferschiefer, Lower Rhine Basin,
984 north-west Germany) from free and S-bound lipids. Organic Geochemistry 25, 131-147.
985 Grice, K., Schouten, S., Peters, K.E., Damste, J.S.S., 1998. Molecular isotopic characterisation of
986 hydrocarbon biomarkers in Palaeocene-Eocene evaporitic, lacustrine source rocks from the Jianghan
987 Basin, China. Organic Geochemistry 29, 1745-1764.
988 Grotheer, H., Robert, A.M., Greenwood, P.F., Grice, K., 2015. Stability and hydrogenation of
989 polycyclic aromatic hydrocarbons during hydropyrolysis (HyPy) - Relevance for high maturity organic
990 matter. Organic Geochemistry 86, 45-54.
991 Hall, P.A., McKirdy, D.M., Grice, K., Edwards, D.S., 2014. Australasian asphaltite strandings: Their
992 origin reviewed in light of the effects of weathering and biodegradation on their biomarker and
993 isotopic profiles. Marine and Petroleum Geology 57, 572-593.
994 Hayes, J.M., Freeman, K.H., Popp, B.N., Hoham, C.H., 1990. COMPOUND-SPECIFIC ISOTOPIC
995 ANALYSES - A NOVEL TOOL FOR RECONSTRUCTION OF ANCIENT BIOGEOCHEMICAL PROCESSES.
996 Organic Geochemistry 16, 1115-1128.

997 Hughes, W.B., Holba, A.G., Dzou, L.I.P., 1995. The ratios of dibenzothiophene to phenanthrene and
998 pristane to phytane as indicators of depositional environment and lithology of petroleum source
999 rocks. Geochim. Cosmochim. Acta 59, 3581-3598.
1000 Jenkyns, H.C., 2010. Geochemistry of oceanic anoxic events. Geochemistry, Geophysics, Geosystems
1001 11.
1002 Jiang, A.Z., Zhou, P.Y., Sun, Y.G., Xie, L.J., 2013. Rapid column chromatography separation of
1003 alkylnaphthalenes from aromatic components in sedimentary organic matter for compound specific
1004 stable isotope analysis. Org. Geochem. 60, 1-8.
1005 Lewan, M.D., 1984. Factors controlling the proportionality of vanadium to nickel in crude oils.
1006 Geochim. Cosmochim. Acta 48, 2231-2238.
1007 Li, Y., Xiong, Y., Chen, Y., Tang, Y., 2014. The effect of evaporation on the concentration and
1008 distribution of diamondoids in oils. Org. Geochem. 69, 88-97.
1009 Long, J.A., Large, R.R., Lee, M.S.Y., Benton, M.J., Danyushevsky, L.V., Chiappe, L.M., Halpin, J.A.,
1010 Cantrill, D., Lottermoser, B., 2016. Severe selenium depletion in the Phanerozoic oceans as a factor
1011 in three global mass extinction events. Gondwana Research 36, 209-218.
1012 Love, G.D., McAulay, A., Snape, C.E., Bishop, A.N., 1997. Effect of process variables in catalytic
1013 hydropyrolysis on the release of covalently bound aliphatic hydrocarbons from sedimentary organic
1014 matter. Energy & Fuels 11, 522-531.
1015 Love, G.D., Snape, C.E., Carr, A.D., Houghton, R.C., 1996. Changes in molecular biomarker and bulk
1016 carbon skeletal parameters of vitrinite concentrates as a function of rank. Energy & Fuels 10, 149-
1017 157.
1018 Ludwig, K.R., 2003. User's manual for Isoplot 3.00. A geochronological toolkit for Microsoft Excel.
1019 Berkeley Geochronology Center Special Publication 4.
1020 Markey, R., Stein, H.J., Hannah, J.L., Georgiev, S.V., Pedersen, J.H., Dons, C.E., 2017. Re-Os
1021 identification of glide faulting and precise ages for correlation from the Upper Jurassic Hekkingen
1022 Formation, southwestern Barents Sea. Palaeogeography Palaeoclimatology Palaeoecology 466, 209-
1023 220.
1024 Maslen, E., Grice, K., Dawson, D., Wang, S., Horsfield, B., 2012. Stable hydrogen isotopes of
1025 isoprenoids and n-alkanes as a proxy for estimating the thermal history of sediments through
1026 geological time. In: Harris, N.B., Peters, K.E. (eds.). Analyzing the Thermal History of Sedimentary
1027 Basins: Methods and Case Studies. Society for Sedimentary Geology Special Publication 103, pp. 29–
1028 43.
1029 Maslen, E., Grice, K., Le Metayer, P., Dawson, D., Edwards, D., 2011. Stable carbon isotopic
1030 compositions of individual aromatic hydrocarbons as source and age indicators in oils from western
1031 Australian basins. Organic Geochemistry 42, 387-398.
1032 Meredith, W., Snape, C.E., Carr, A.D., Nytoft, H.P., Love, G.D., 2008. The occurrence of unusual
1033 hopenes in hydropyrolysates generated from severely biodegraded oil seep asphaltenes. Organic
1034 Geochemistry 39, 1243-1248.
1035 Nelson, R.K., Aeppli, C., Samuel, J., Chen, H., de Oliveira, A.H.B., Eiserbeck, C., Frysinger, G.S., Gaines,
1036 R.B., Grice, K., Gros, J., Hall, G.J., Koolen, H.H.F., Lemkau, K.L., McKenna, A.M., Reddy, C.M., Rodgers,
1037 R.P., Swarthout, R.F., Valentine, D.L., White, H.K., 2016. Applications of comprehensive two-
1038 dimensional gas chromatography (GC × GC) in studying the source, transport, and fate of petroleum
1039 hydrocarbons in the environment, in: Stout, S.A., Wang, Z. (Eds.), Standard Handbook Oil Spill
1040 Environmental Forensics Fingerprinting and Source Identification, 2nd ed. Academic Press,
1041 Cambridge, MA, USA.
1042 NRC, 2003. Oil in the Sea III: Inputs, Fates and Effects. National Research Council (US). National
1043 Academies Press, Washington, DC, p. 280.
1044 Padley, D., 1995. Petroleum geochemistry of the Otway Basin and the significance of coastal
1045 bitumen strandings on adjacent southern Australian beaches.
1046 Peters, K.E., Moldowan, J.M., 1993. The Biomarker Guide. Interpreting Molecular Fossils in
1047 Petroleum and Ancient Sediments. Prentice-Hall, New Jersey.

Peters, K.E., Walters, C.C., Moldowan, J.M., 2007. Biomarkers and Isotopes in Petroleum Systems and Earth History, 2nd Edition ed. Cambridge University Press, Cambridge, UK.
Reinhardt, M., Duda, J.P., Blumenberg, M., Ostertag-Henning, C., Reitner, J., Heim, C., Thiel, V., 2018. The taphonomic fate of isorenieratene in Lower Jurassic shales-controlled by iron? Geobiology 16, 237-251.
Robson, J.N., Rowland, S.J., 1993. Synthesis, chromatographic and spectral characterization of 2,6,11,15-tetramethylhexadecane (crocetane) and 2,6,9,13-tetramethyltetradecane - reference acyclic isoprenoids for geochemical studies. Organic Geochemistry 20, 1093-1098.
Scarlett, A.G., Clough, R., West, C., Lewis, C.A., Booth, A.M., Rowland, S.J., 2011. Alkylnaphthalenes: Priority Pollutants or Minor Contributors to the Poor Health of Marine Mussels? Environmental Science & Technology 45, 6160-6166.
Schwark, L., Frimmel, A., 2004. Chemostratigraphy of the Posidonia Black Shale, SW-Germany II. Assessment of extent and persistence of photic-zone anoxia using aryl isoprenoid distributions. Chemical Geology 206, 231-248.
Selby, D., Creaser, R.A., 2005. Direct Radiometric Dating of Hydrocarbon Deposits Using Rhenium-Osmium Isotopes. Science 308, 1293.
Selby, D., Creaser, R.A., Fowler, M.G., 2007. Re-Os elemental and isotopic systematics in crude oils. Geochim. Cosmochim. Acta 71, 378-386.
Sessions, A.L., 2016. Factors controlling the deuterium contents of sedimentary hydrocarbons. Organic Geochemistry 96, 43-64.
Song, D.F., He, D.F., Qi, X.F., Wang, S.R., Li, D., 2015. Occurrence and composition of solid bitumens from the Bulonggoer Devonian paleo-oil reservoir, North Xinjiang, China. Organic Geochemistry 83-84, 1-15.
Sonibare, O.O., Snape, C.E., Meredith, W., Uguna, C.N., Love, G.D., 2009. Geochemical characterisation of heavily biodegraded tar sand bitumens by catalytic hydropyrolysis. Journal of Analytical and Applied Pyrolysis 86, 135-140.
Spaak, G., Nelson, R.K., Reddy, C.M., Scarlett, A.G., Chidlow, G.E., Grice, K., 2016. Advances on the separation of crocetane and phytane using GC–MS and GC×GC–TOFMS. Organic Geochemistry 98, 176-182.
Tang, T., Mohr, W., Sattin, S.R., Rogers, D.R., Girguis, P.R., Pearson, A., 2017. Geochemically distinct carbon isotope distributions in Allochromatium vinosum DSM 180(T) grown photoautotrophically and photoheterotrophically. Geobiology 15, 324-339.
Tejada, M.L.G., Suzuki, K., Kuroda, J., Coccioni, R., Mahoney, J.J., Ohkouchi, N., Sakamoto, T., Tatsumi, Y., 2009. Ontong Java Plateau eruption as a trigger for the early Aptian oceanic anoxic event. Geology 37, 855-858.
Totterdell, J., I M Struckmeyer, H., Boreham, C., Mitchell, C., Monteil, E., E Bradshaw, B., 2008. Mid–Late Cretaceous organic-rich rocks from the eastern Bight Basin: implications for prospectivity.
Totterdell, J.M., Mitchell, C.H., 2009. Bight Basin geological sampling and seepage survey, R/V Southern Surveyor Survey SS01/2007: Post-survey report. Australia: Geoscience Australia Record 2009/24.
Turgeon, S.C., Creaser, R.A., 2008. Cretaceous oceanic anoxic event 2 triggered by a massive magmatic episode. Nature 454, 323-U329.
Ventura, G.T., Kenig, F., Reddy, C.M., Frysinger, G.S., Nelson, R.K., Van Mooy, B., Gaines, R.B., 2008. Analysis of unresolved complex mixtures of hydrocarbons extracted from Late Archean sediments by comprehensive two-dimensional gas chromatography (GCxGC). Organic Geochemistry 39, 846-867.
Wang, Z., Stout, S.A., Fingas, M., 2006. Forensic Fingerprinting of Biomarkers for Oil Spill Characterization and Source Identification. Environmental Forensics 7, 105-146.
Whiteside, J.H., Grice, K., 2016. Biomarker Records Associated with Mass Extinction Events. Annual Review of Earth and Planetary Sciences 44, 581-612.

1098

Table and Figure legends

Table 1 Asphaltite identification, weathering description, location and year of collection.

Table 2 Concentrations (µg g^{-1}) of elements in asphaltites. Data for additional elements with low concentrations are provided in Table S1.

Table 3. Re-Os concentration and isotopic data for asphaltites, Otway and Bight basins, South Australia

Fig. 1 Locations of asphaltite strandings and sedimentary basins; further details available in Table 1.

Fig.2 Classification of GC×GC-TOFMS chromatographic peaks for the asphaltite sample 85; maltene and asphaltene hydropyrolysates based on the relative number of peaks and on peak area within the saturated (A and B respectively) and aromatic (C and D respectively) hydrocarbon fractions.

Fig. 3 Comparison of steranes (GC-MS fragmentogram *m/z* 217) present in (A) maltene and (B) asphaltene hydropyrolysate of asphaltite sample 305.

Fig. 4 Comparison of hopanes (GC-MS fragmentogram *m/z* 191) present in (A) maltene and (B) asphaltene hydropyrolysate of asphaltite sample 305.

Fig. 5 Crossplot of mean $\delta^{13}C$ and $\delta^{2}H$ for *n*-alkanes (*n*-C_{17} and *n*-C_{18}) and the isoprenoids pristane (Pr) and phytane (Ph) in asphaltites. Error bars = 95 % confidence limits.

Fig. 6 Mean $\delta^{2}H$ values for *n*-alkanes and isoprenoids pristane (Pr) and phytane (Ph) for four asphaltite samples, 306 (A), MH1 (B), 305 (C), and CL1 (D). Error bars represent standard deviation (n = 3).

Fig. 7 Rhenium-osmium (Re-Os) isochron plot for asphaltene derived from five asphaltite samples in this study (filled red ellipses, see Table 3). Sixteen open ellipses (74 ± 26 Ma)

are from Corrick et al. (2019) with nine blue ellipses selected to report a Re-Os age of 68 ± 15 Ma. Seven gray ellipses represent samples selectively removed from their 16-sample data set (34 ± 83 Ma), noting that the gray ellipses are much closer to the data we acquired from the same sample region. Eight samples from the Corrick et al. (2019) study, including 6 gray ellipses they label as outliers and 2 of the 9 blue ellipses preferred by the authors, plot on the isochron line in this study. For example, regression of our data with the lowermost left point from the Corrick et al (2019) study yields a 6-point isochron age with an improved uncertainty (104 ± 12 Ma equal to the 103 ± 22 Ma age derived from our 5-point isochron (this study). Both regressions give a reasonable probability of fit. See text for further discussion.

Appendix

Abbreviations

CPI	Carbon preference index
CSIA	Compound specific isotope analysis
GC×GC-TOFMS	Comprehensive two-dimensional gas chromatography – time of flight mass spectrometry
GC-irMS	Gas chromatography isotope-ratio mass spectrometry
GC-MS	Gas chromatography–mass spectrometry
HyPy	High pressure hydropyrolysis
ICP-MS	Inductively coupled plasma-mass spectrometry
OEP	Odd-over-even predominance index(DE insert definition)
MDI	Methyldiamantane index = 4-MD/(4-MD +1-MD + 3-MD)
MSWD	Mean square weighted deviation
xMD	1, 3 or 4-methyldiamantane
MPI-1	Methylphenanthrene index 1(MPI-1) = 1.5(2-MP + 3-MP)/(P + 1-MP + 9-MP)
MPR	Methylphenanthrene ratio = 2-MP/1-MP
MRM	Multiple reaction monitoring
xMP	1, 2, 3 or 9-methylphenanthrene
n-C_x	Normal-alkane $C_{\text{carbon number}}$

PAH	Polycyclic aromatic hydrocarbon
Ph	Phytane
Pr	Pristane
PZE	Photic zone euxinia
Rc	Calculated vitrinite reflectance (Rc) % = 0.6(MPI-1) + 0.4
Re-Os	Rhenium-osmium ratio
SAR	Saturated, aromatic and resin fractions
UCM	Unresolved complex mixture

1137

1138

1139

1140

1141

1142

1143

1144

1145

1146

1147

1148

1149

1150

1151

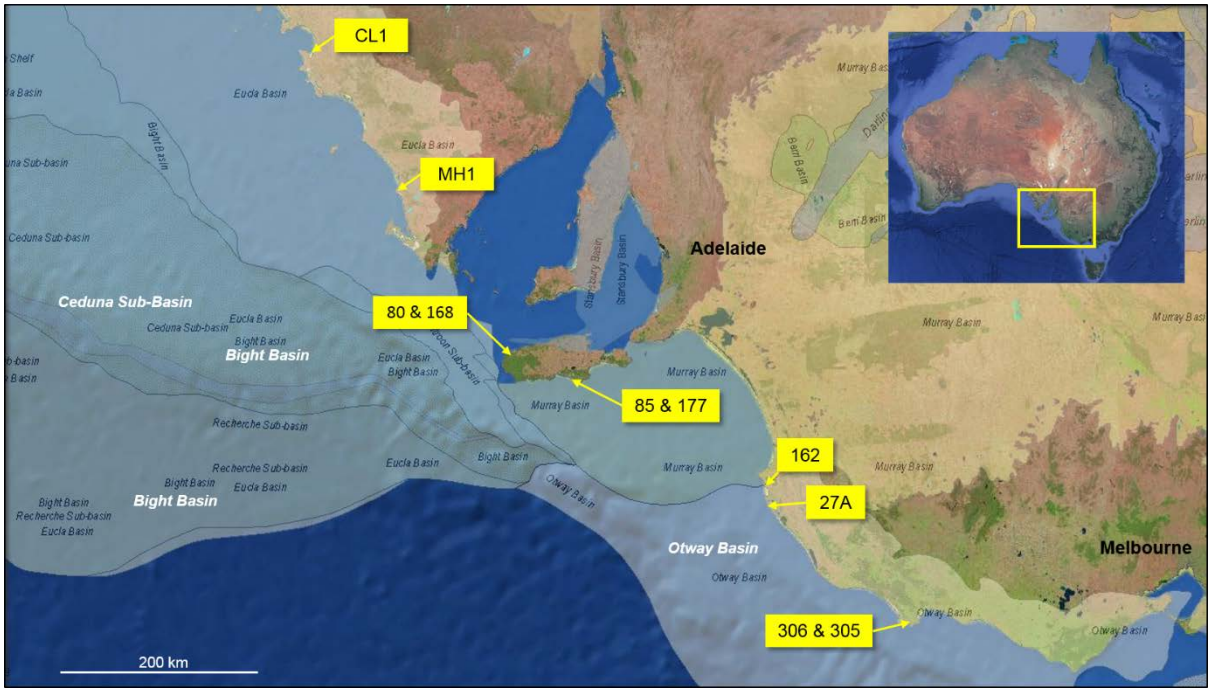
CL1
MH1
80 & 168
85 & 177
162
27A
306 & 305
Adelaide
Melbourne
Ceduna Sub-Basin
Bight Basin
Otway Basin
Eucla Basin
Murray Basin
Recherche Sub-basin
200 km

Fig. 1

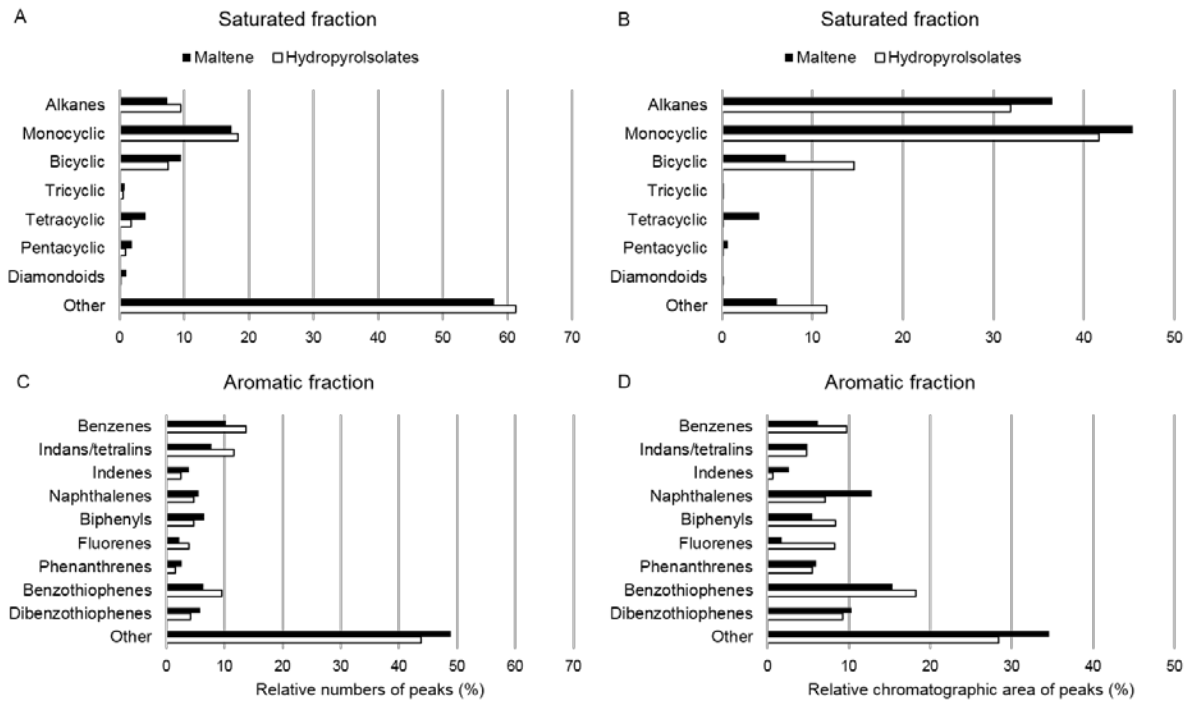
A
Saturated fraction
Maltene
Hydropyrolsolates
Alkanes
Monocyclic
Bicyclic
Tricyclic
Tetracyclic
Pentacyclic
Diamondoids
Other
0
10
20
30
40
50
60
70
B
Saturated fraction
Maltene
Hydropyrolsolates
Alkanes
Monocyclic
Bicyclic
Tricyclic
Tetracyclic
Pentacyclic
Diamondoids
Other
0
10
20
30
40
50
C
Aromatic fraction
Benzenes
Indans/tetralins
Indenes
Naphthalenes
Biphenyls
Fluorenes
Phenanthrenes
Benzothiophenes
Dibenzothiophenes
Other
0
10
20
30
40
50
60
70
Relative numbers of peaks (%)
D
Aromatic fraction
Benzenes
Indans/tetralins
Indenes
Naphthalenes
Biphenyls
Fluorenes
Phenanthrenes
Benzothiophenes
Dibenzothiophenes
Other
0
10
20
30
40
50
Relative chromatographic area of peaks (%)

Fig. 2

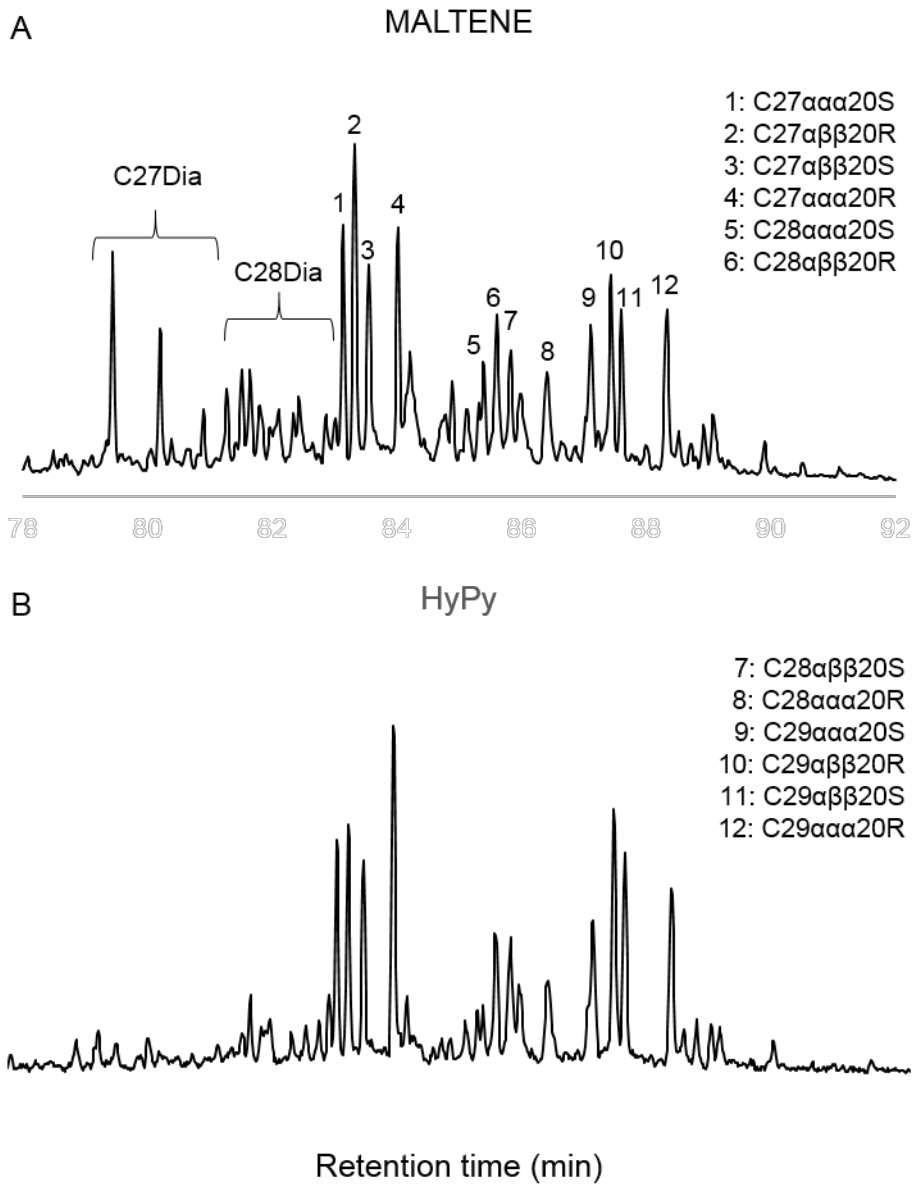
A
MALTENE
1: C27ααα20S
2: C27αββ20R
3: C27αββ20S
4: C27ααα20R
5: C28ααα20S
6: C28αββ20R
C27Dia
C28Dia
1
2
3
4
5
6
7
8
9
10
11
12
78
80
82
84
86
88
90
92
B
HyPy
7: C28αββ20S
8: C28ααα20R
9: C29ααα20S
10: C29αββ20R
11: C29αββ20S
12: C29ααα20R
Retention time (min)

Fig. 3

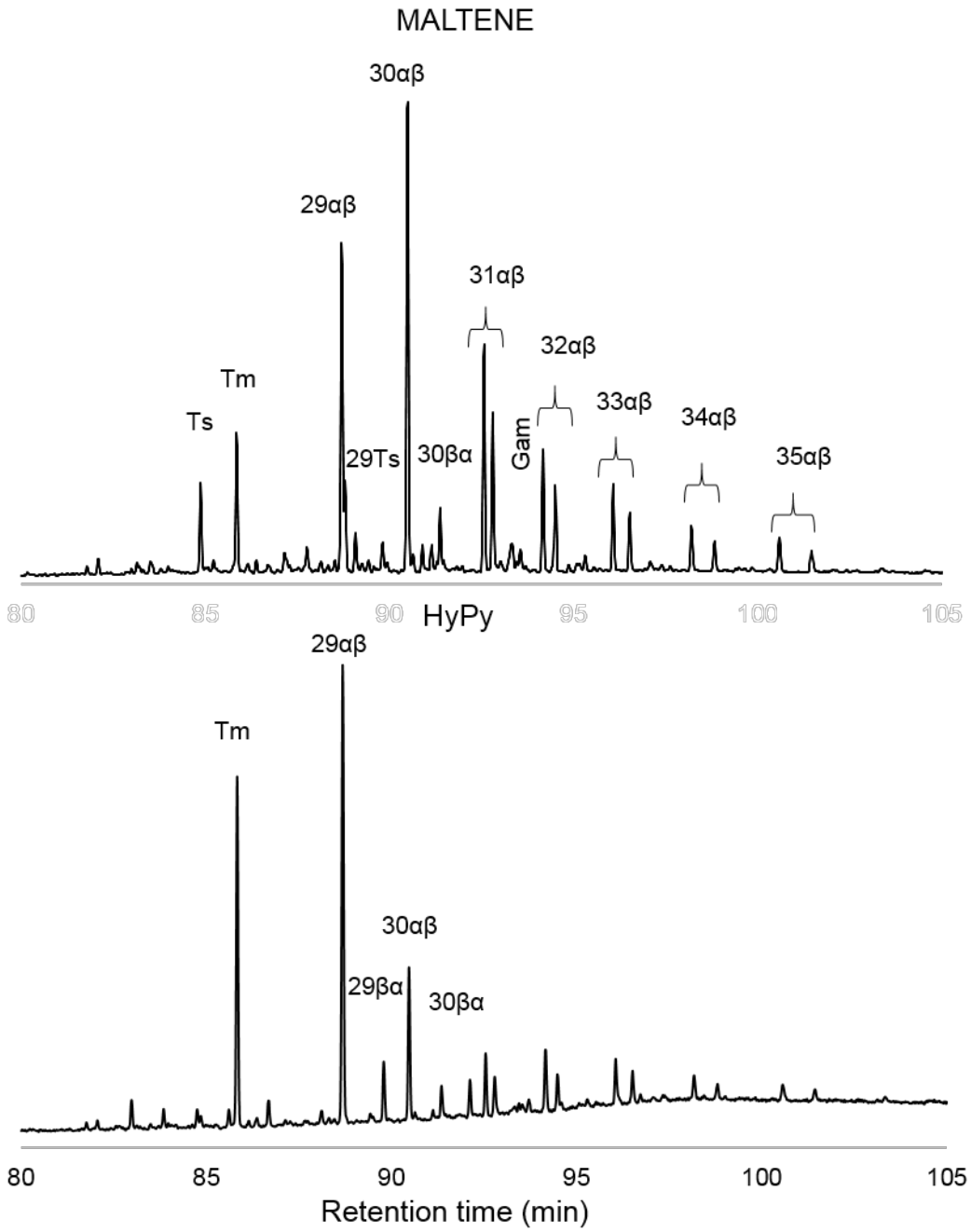
MALTENE
30αβ
29αβ
31αβ
32αβ
Tm
Ts
33αβ
34αβ
29Ts
30βα
Gam
35αβ
80
85
90
HyPy
95
100
105
29αβ
Tm
30αβ
29βα
30βα
80
85
90
95
100
105
Retention time (min)

Fig. 4

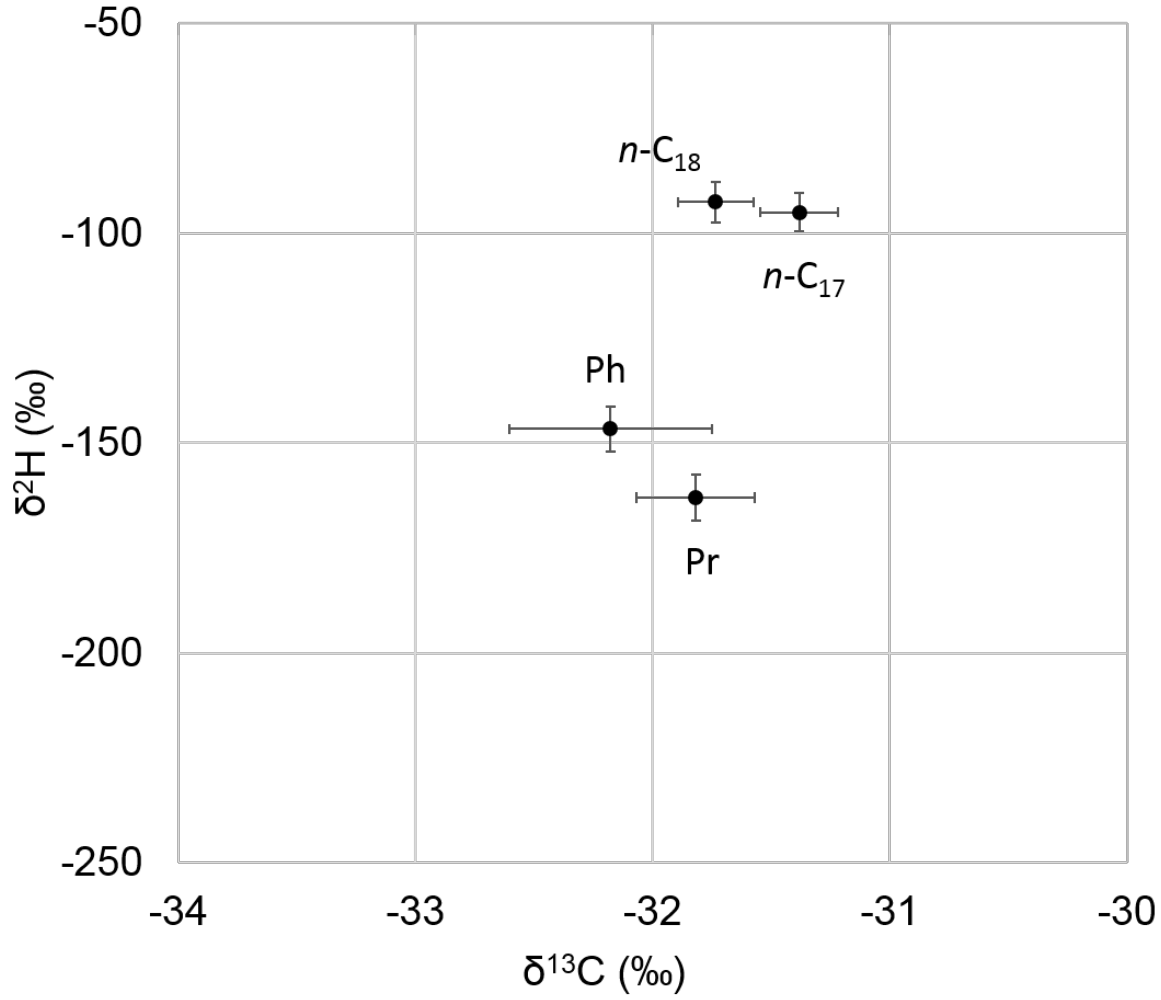

Fig. 5

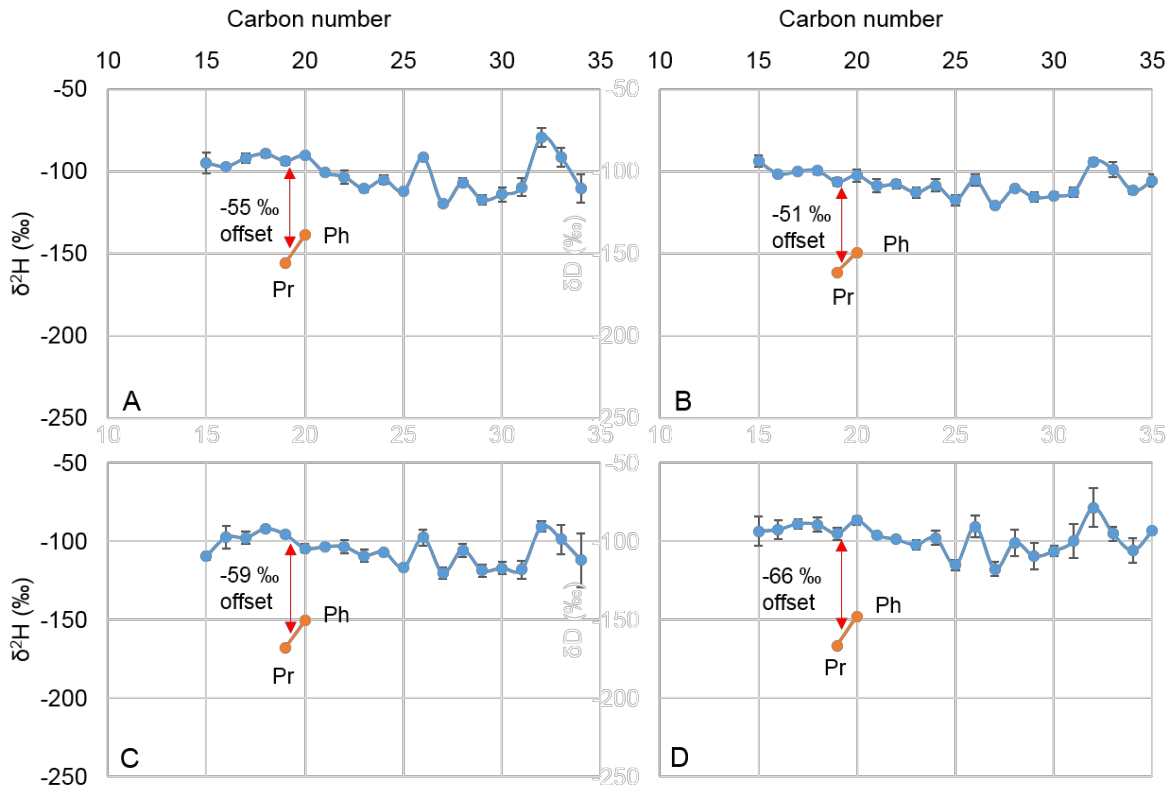
Carbon number
10
15
20
25
30
35
-50
-100
-150
-200
-250
δ²H (‰)
δD (‰)
-55 ‰
offset
Ph
Pr
A
-51 ‰
offset
Ph
Pr
B
-59 ‰
offset
Ph
Pr
C
-66 ‰
offset
Ph
Pr
D

Fig. 6

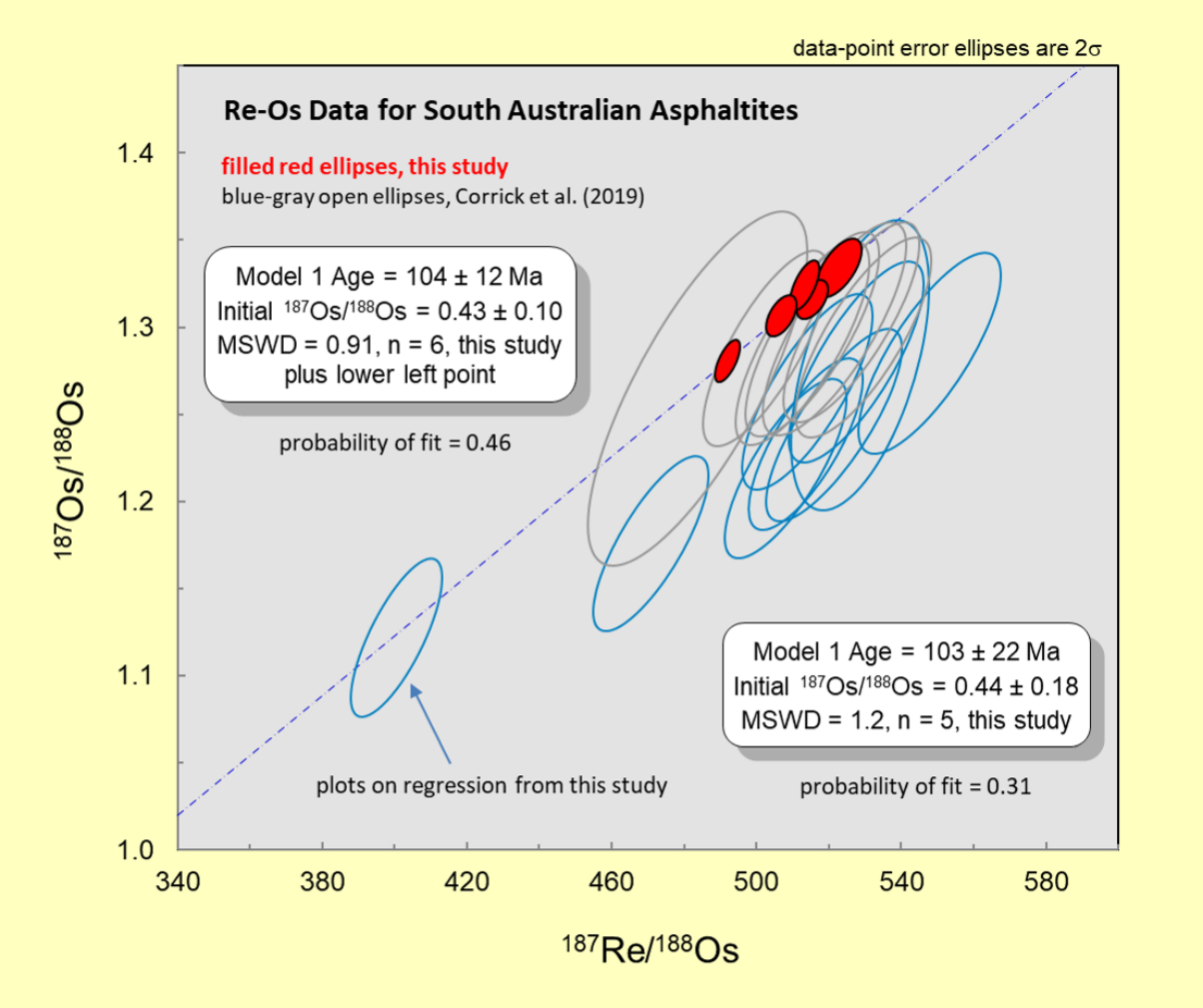
data-point error ellipses are 2σ
Re-Os Data for South Australian Asphaltites
filled red ellipses, this study
blue-gray open ellipses, Corrick et al. (2019)
Model 1 Age = 104 ± 12 Ma
Initial 187Os/188Os = 0.43 ± 0.10
MSWD = 0.91, n = 6, this study
plus lower left point
probability of fit = 0.46
Model 1 Age = 103 ± 22 Ma
Initial 187Os/188Os = 0.44 ± 0.18
MSWD = 1.2, n = 5, this study
probability of fit = 0.31
plots on regression from this study
187Os/188Os
187Re/188Os
1.0
1.1
1.2
1.3
1.4
340
380
420
460
500
540
580

Fig. 7

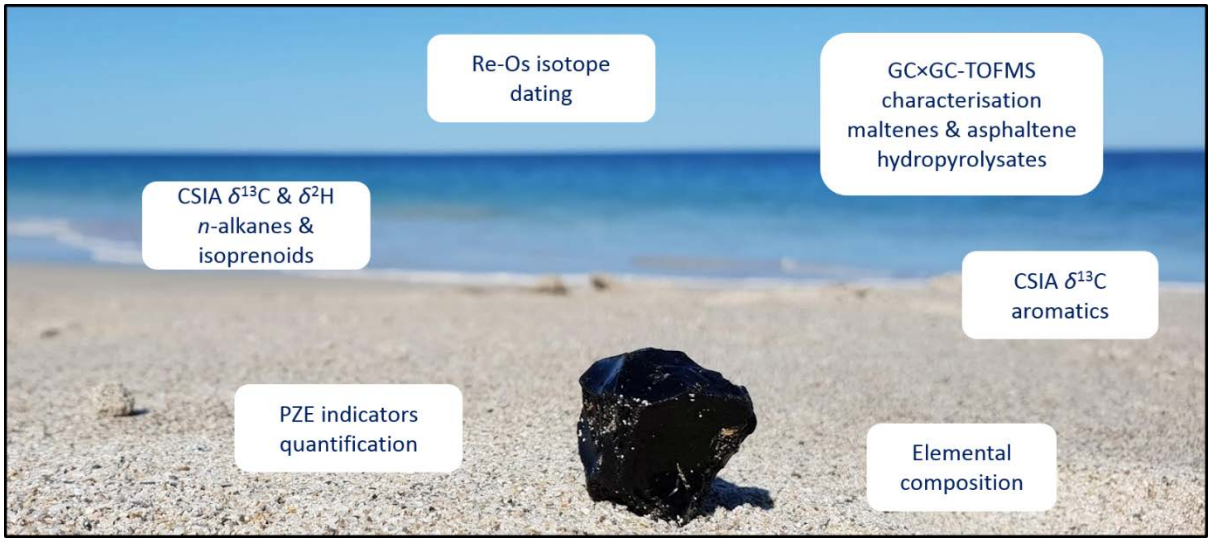

Graphical abstract

For submission to Organic Geochemistry

Supplementary Information

Multi-spectroscopic and elemental characterization of southern Australian asphaltites

Alan G. Scarlett[a*], Alex I. Holman[a], Svetoslav V. Georgiev[b], Holly J. Stein[b,c], Roger E. Summons[d], and Kliti Grice[a*]

[a] Western Australian Organic and Isotope Geochemistry Centre, The Institute for Geoscience Research, School of Earth and Planetary Sciences, Curtin University, Western Australia

[b] AIRIE Program, Colorado State University, Fort Collins, 80523-1482 CO, USA

[c] Geosciences, University of Oslo, Norway

[d] Department of Earth, Atmospheric and Planetary Sciences, Massachusetts Institute of Technology, 77 Massachusetts Avenue, Cambridge, MA 02139, USA

Corresponding author: * alan.scarlett@curtin.edu.au, K.Grice@curtin.edu.au (post publication only)

Table S1 Concentrations (µg g^{-1}) of elements in asphaltites with very low abundance not shown in Table 2. Additional elements thorium, antinomy, tellurium, cesium, praseodymium, neodymium, samarium, europium, gadolinium, terbium, dysprosium, holmium, erbium, thulium, ytterbium, lutetium, hafnium, tantalum, mercury and thallium were all below detection limits of 0.1 mg g^{-1} asphaltite and are not shown.

Asphaltite	**Li**	**Sc**	**Co**	**Ga**	**As**	**Rb**	**Zr**	**Sn**	**Ba**	**La**	**Ce**	**U**	**Pb**	**Bi**	**Mo**	**Se**
27A	< 0.1	< 0.1	1.0	0.2	< 0.1	< 0.1	0.2	< 0.1	0.3	< 0.1	< 0.1	< 0.1	0.1	< 0.1	0.6	0.1
80	< 0.1	0.5	1.0	0.2	< 0.1	< 0.1	0.2	< 0.1	0.5	< 0.1	< 0.1	< 0.1	0.2	< 0.1	0.6	0.2
85	< 0.1	< 0.1	1.0	0.2	< 0.1	< 0.1	0.3	0.2	2.1	0.1	0.1	< 0.1	0.5	< 0.1	0.7	< 0.1
162	< 0.1	< 0.1	1.0	0.2	< 0.1	0.2	0.2	0.1	2.5	< 0.1	0.1	< 0.1	0.6	< 0.1	0.7	< 0.1
168	0.4	0.2	1.0	0.1	< 0.1	< 0.1	0.2	< 0.1	< 0.1	< 0.1	< 0.1	< 0.1	< 0.1	0.2	0.6	< 0.1
177	1.0	< 0.1	0.9	0.1	< 0.1	< 0.1	0.2	0.7	0.1	0.2	0.2	< 0.1	< 0.1	< 0.1	0.6	< 0.1
305	0.8	1.1	1.0	0.2	< 0.1	< 0.1	0.6	0.1	0.5	0.2	0.2	0.2	0.3	< 0.1	0.7	0.1
306	< 0.1	< 0.1	1.0	0.2	< 0.1	< 0.1	0.2	< 0.1	0.4	< 0.1	< 0.1	< 0.1	0.1	< 0.1	0.7	0.2
CL1	< 0.1	< 0.1	1.0	0.2	0.2	< 0.1	0.4	0.1	1.2	< 0.1	0.1	< 0.1	0.3	< 0.1	0.7	0.2
MH1	1.5	1.8	1.1	0.2	< 0.1	< 0.1	0.5	0.2	0.3	< 0.1	< 0.1	< 0.1	1.0	< 0.1	0.7	0.3

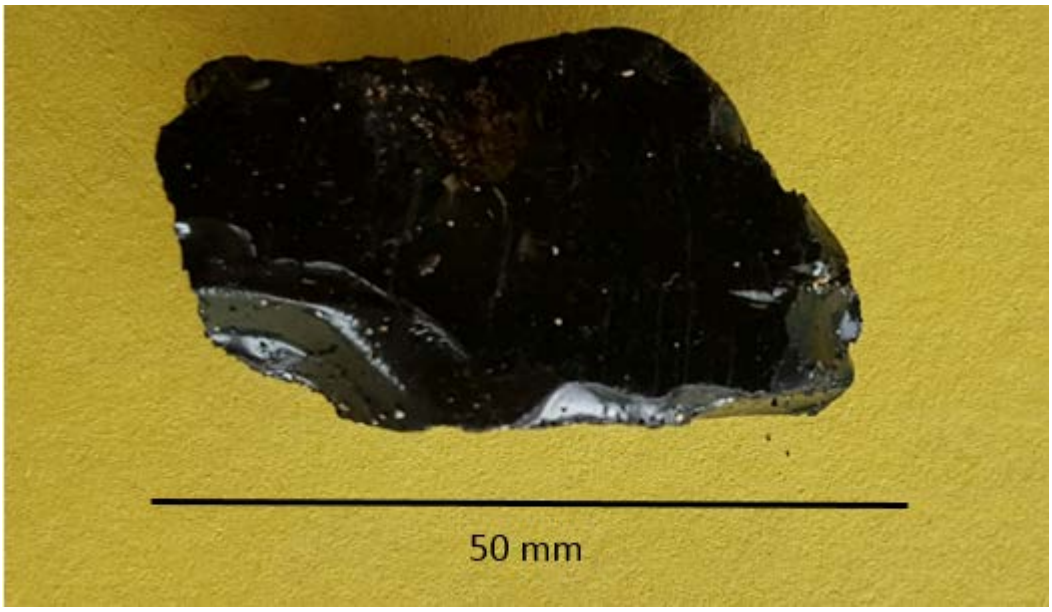

Figure S1. Example of asphaltite appearance (162 shown)

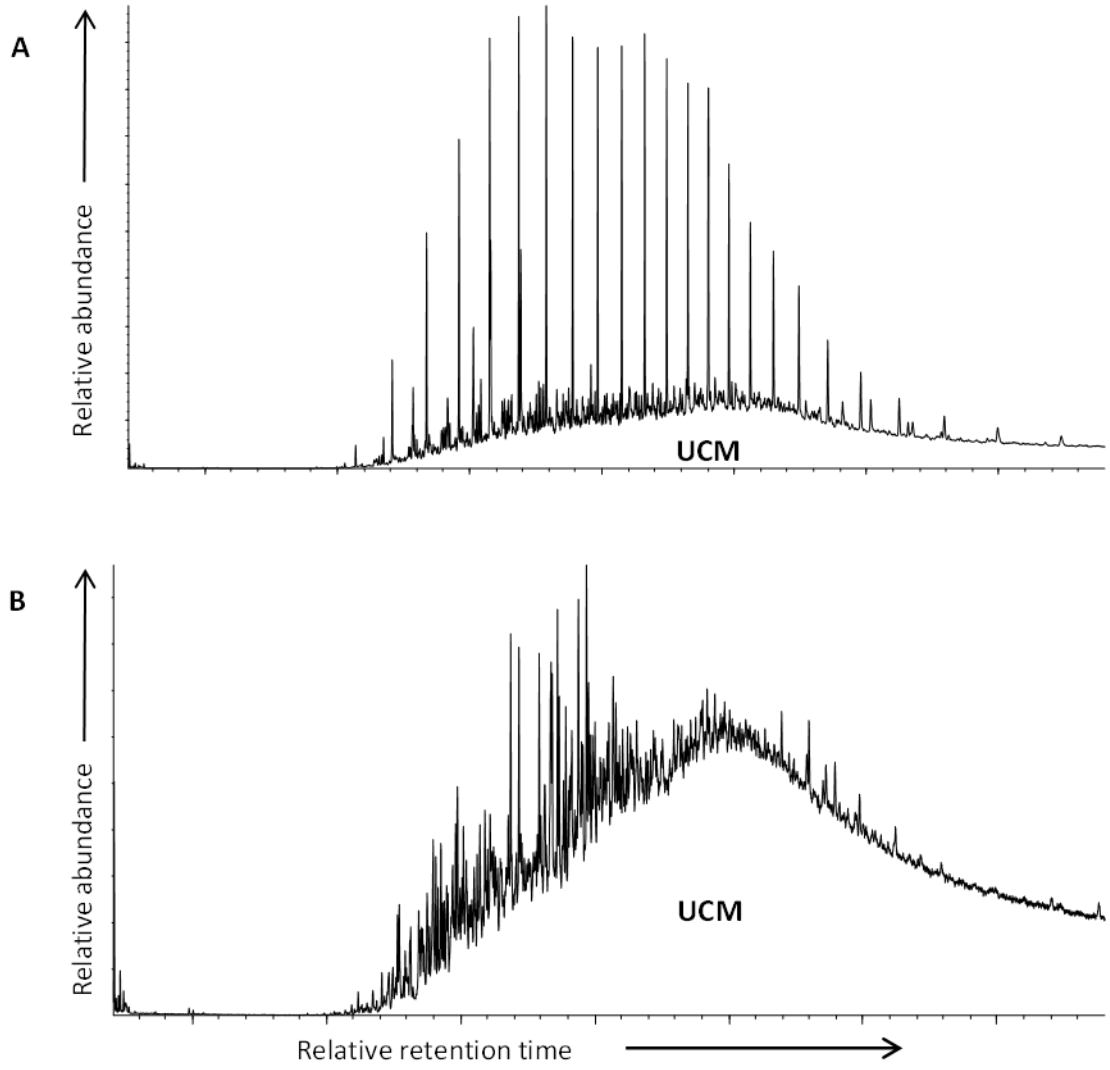

Fig. S2 Example of GC-MS chromatograms of saturates fraction (A) and aromatic fraction (B) of maltenes extracted from an asphaltite (85). Unresolved complex mixtures of hydrocarbons are present in the saturated fracture (A) but more prominent in the aromatics fraction (B).

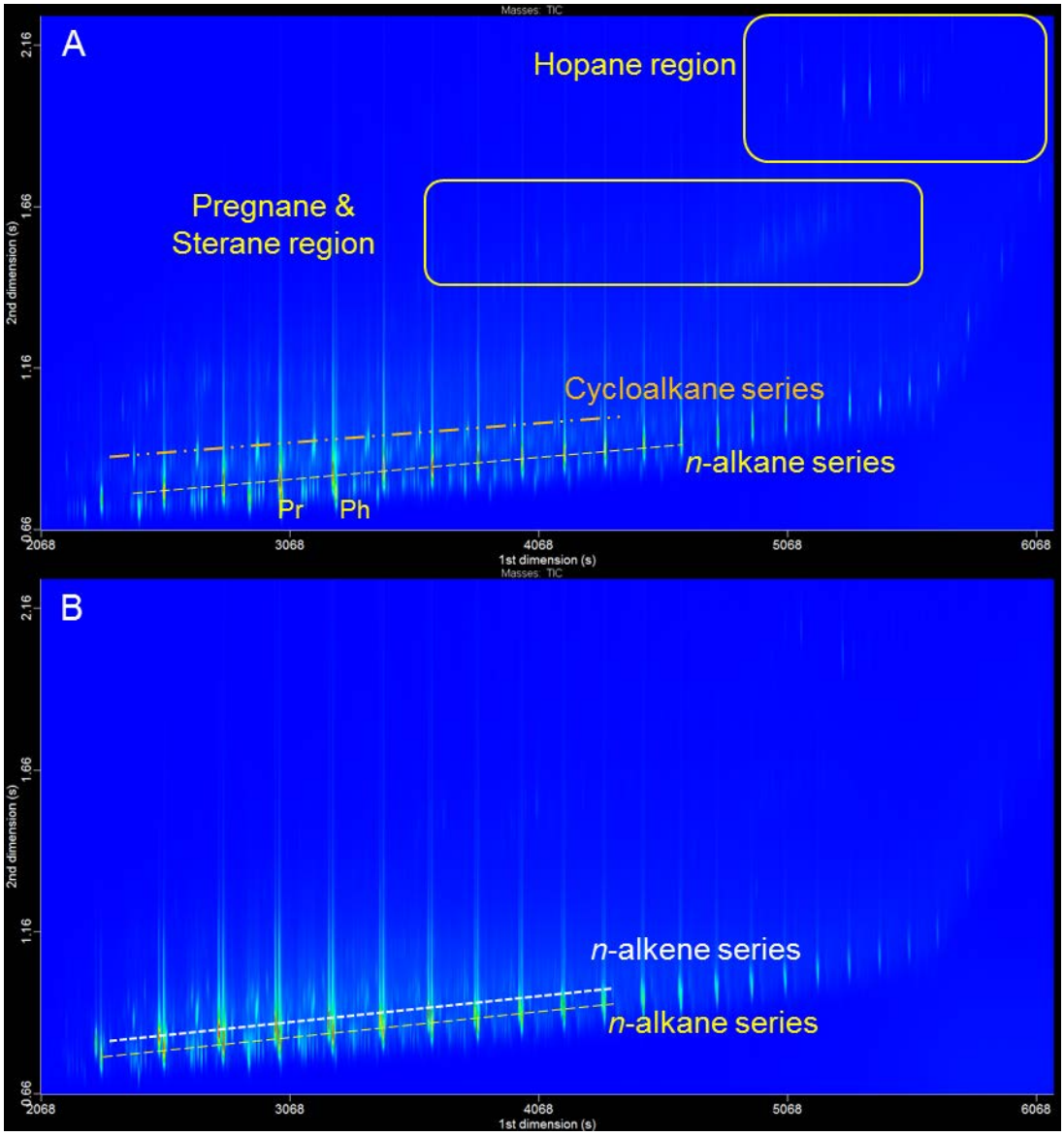

Fig. S3 GC×GC-TOFMS total ion chromatograms of saturated fractions from (A) maltene and (B) hydropyrolysates from asphaltene phase of asphaltite 85 showing the presence of a series of *n*-alkenes in the latter.

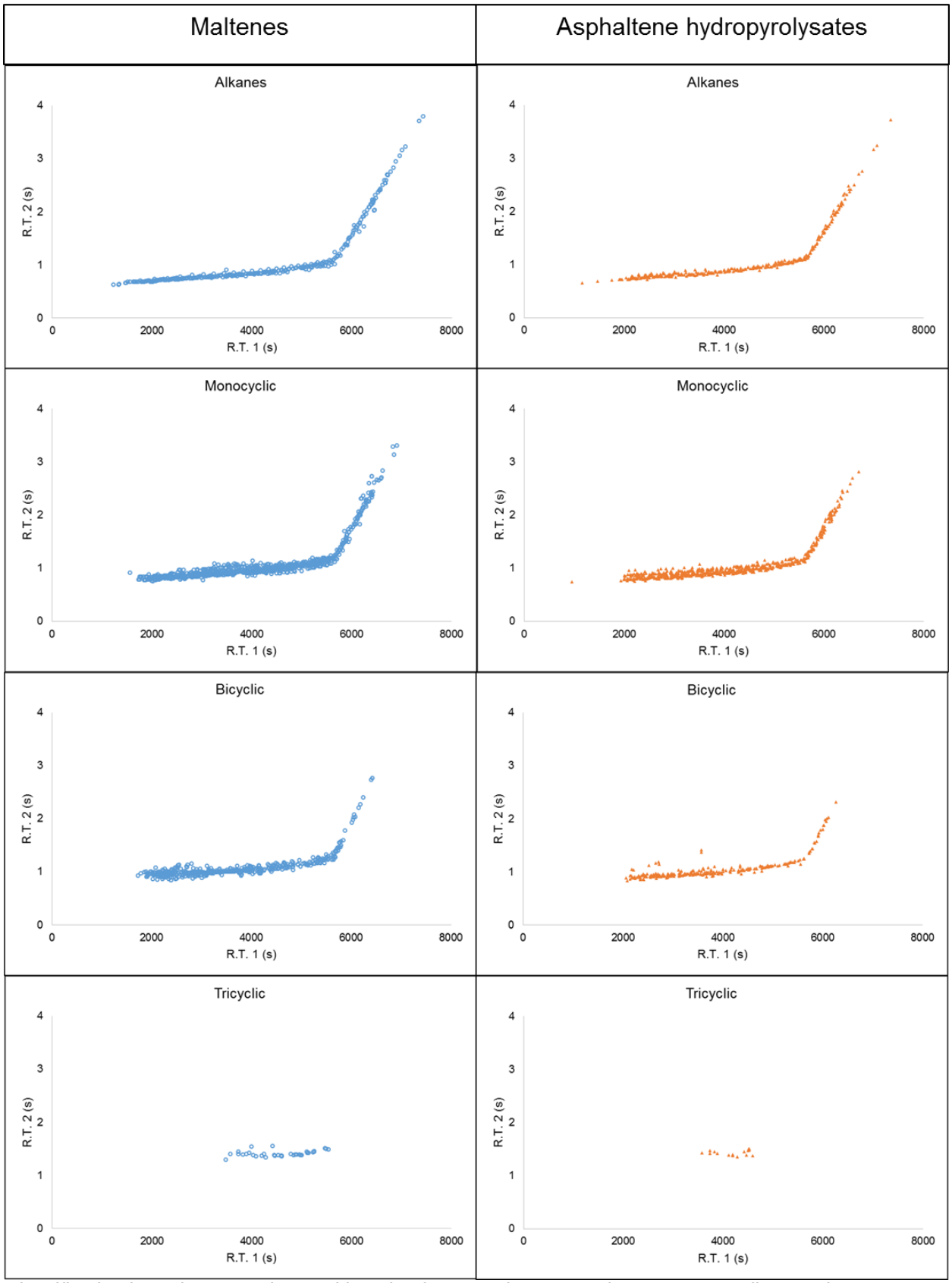

Classification based on retention position plus fragment ions e.g. m/z 57, 71, 85 = alkanes plus retention position.
Peaks classified as column bleed such as siloxanes not shown.

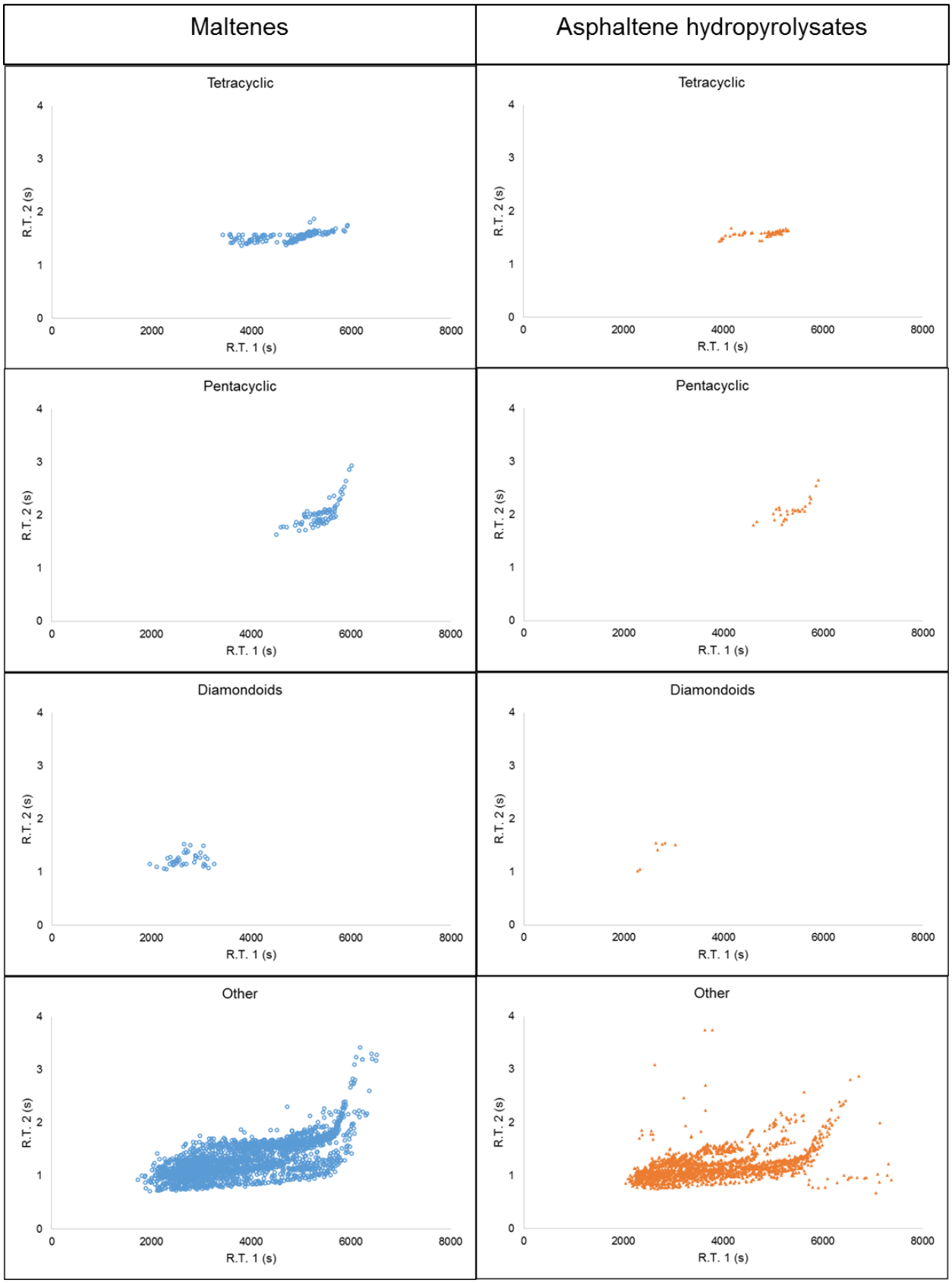

Fig. S4 Elution positions of GC×GC-TOFMS chromatographic peaks of asphaltite 85 saturate fraction classified by mass spectra into major compound groupings commonly found in oils (Fig. 1). Blue open circle (left column) = asphaltite maltenes. Orange triangle (right column) = asphaltene hydropyrolysates. RT1 = 1st dimension (volatility) retention time (s) and RT2 = 2nd dimension (polar) retention time (s).

Maltenes	Asphaltene hydropyrolysates
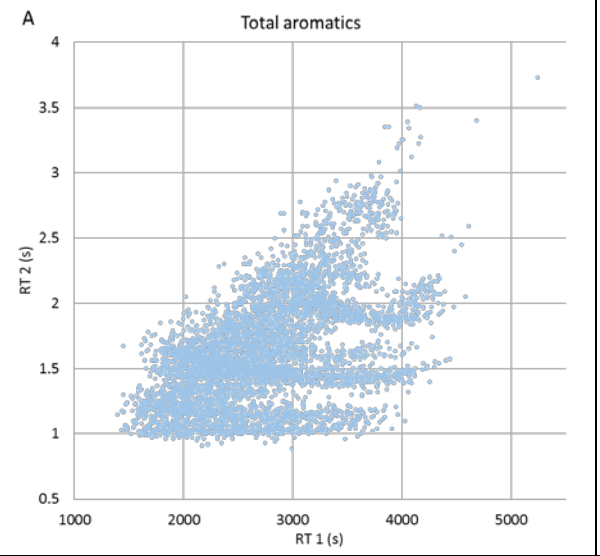	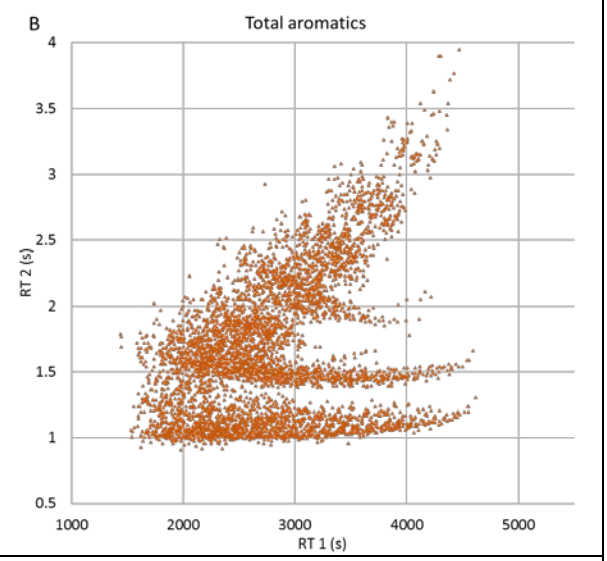
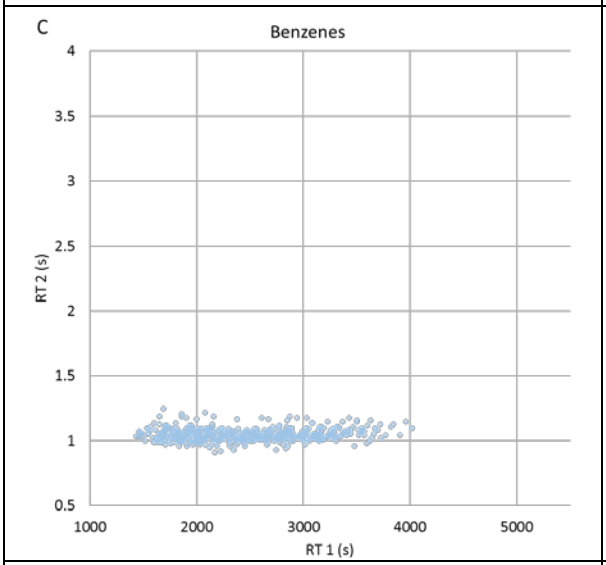	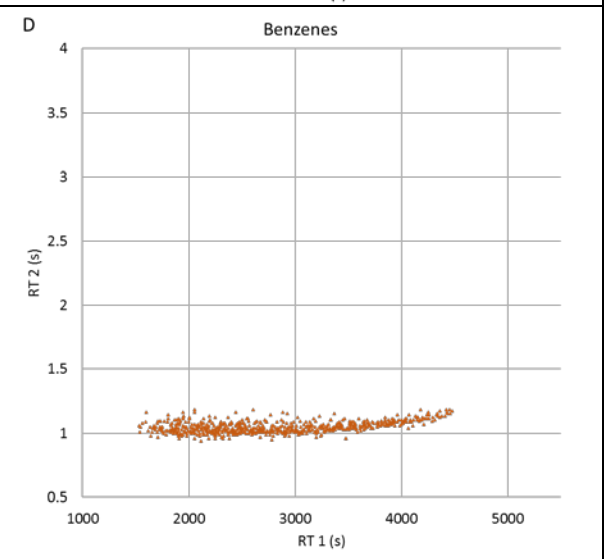
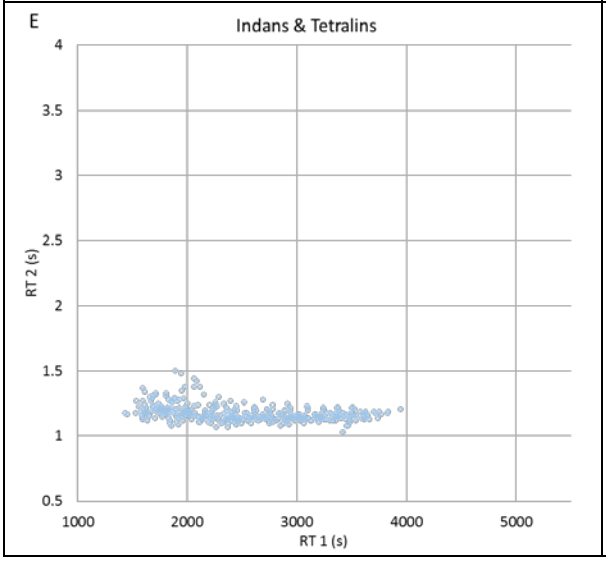	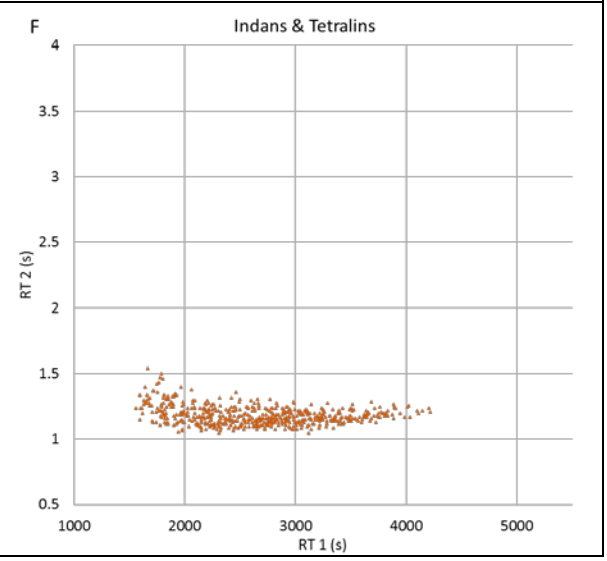

Maltenes	Asphaltene hydropyrolysates
G 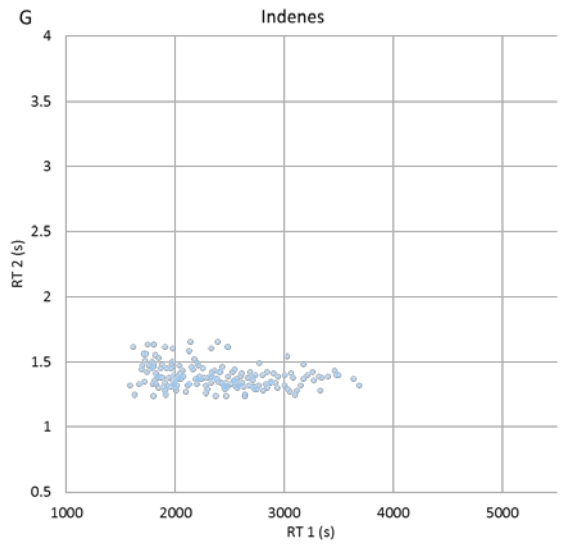	H 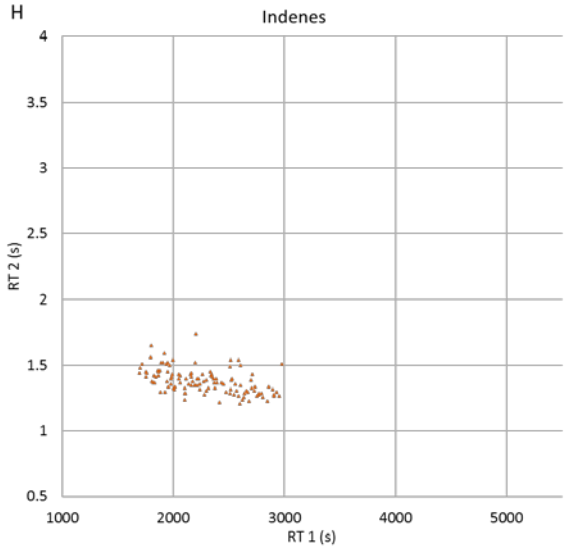
I 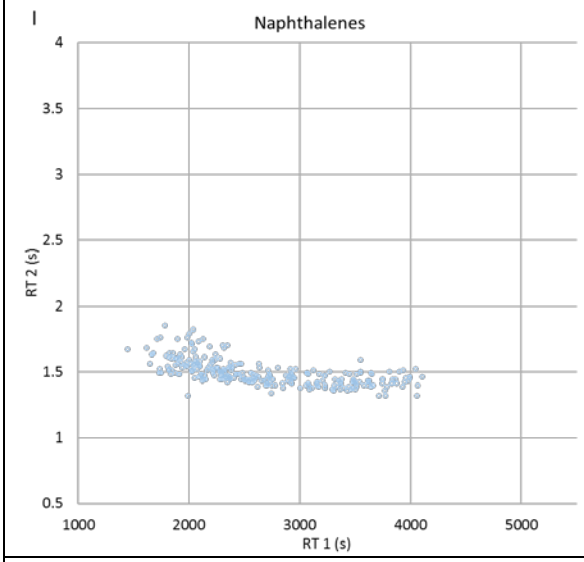	J 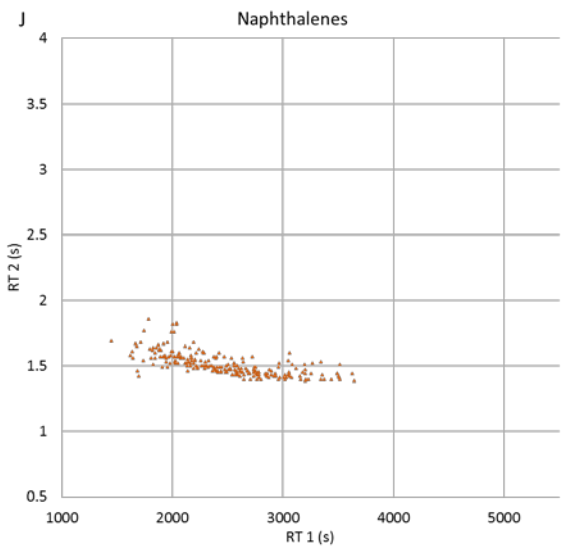
K 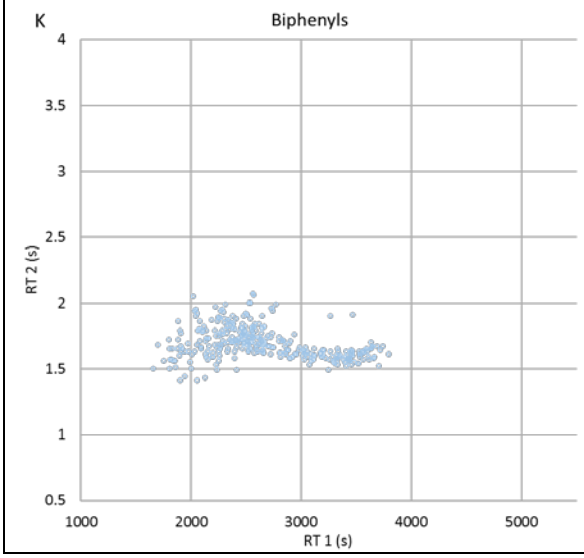	L 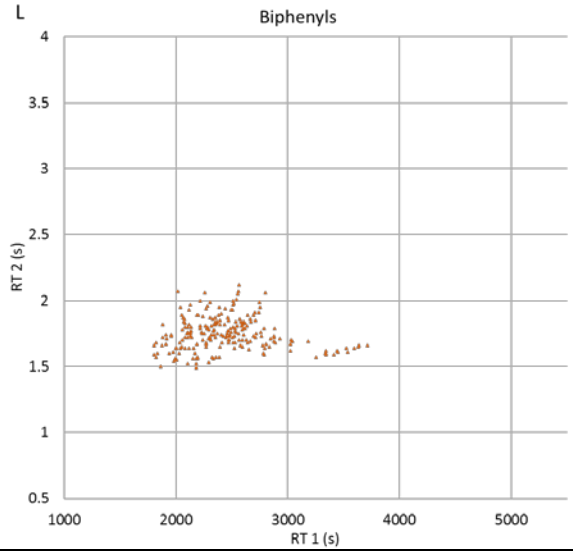

Maltenes	Asphaltene hydropyrolysates
M 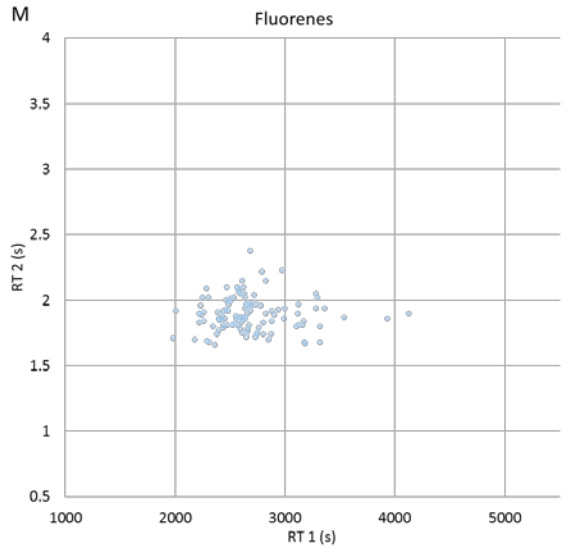	N 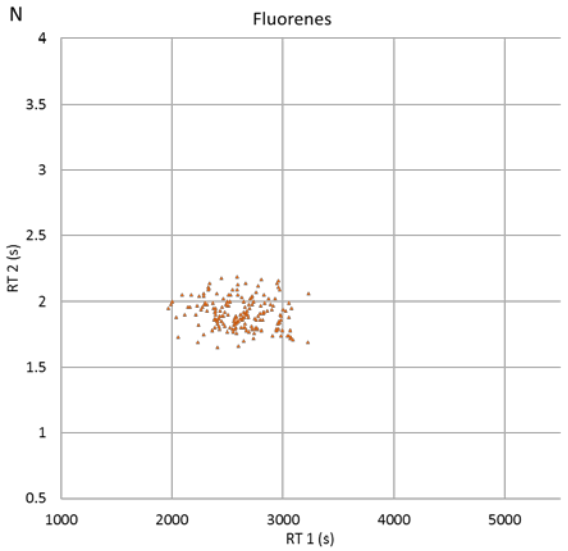
O 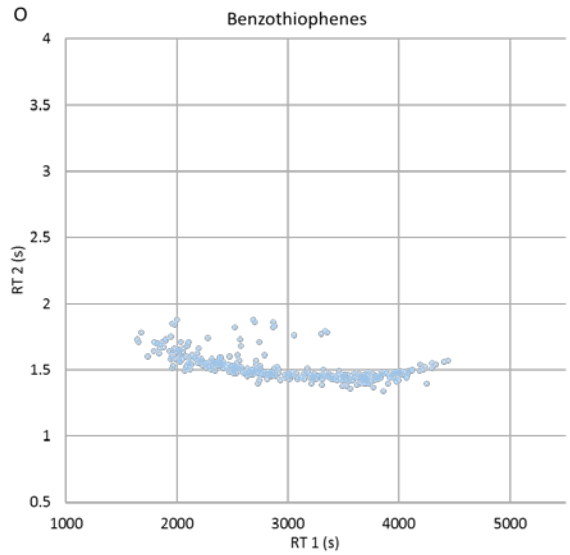	P 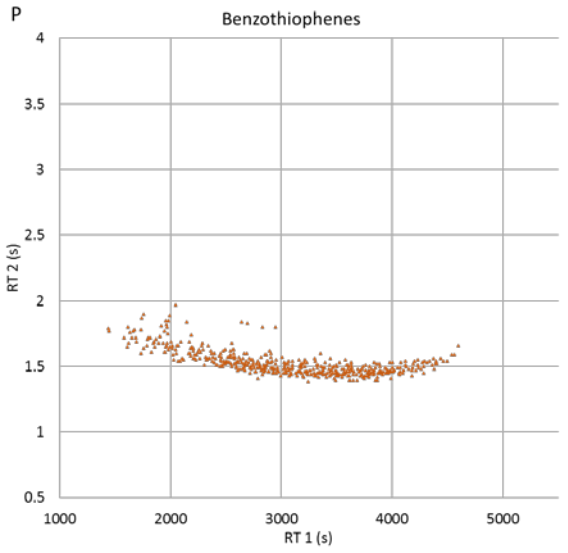
Q 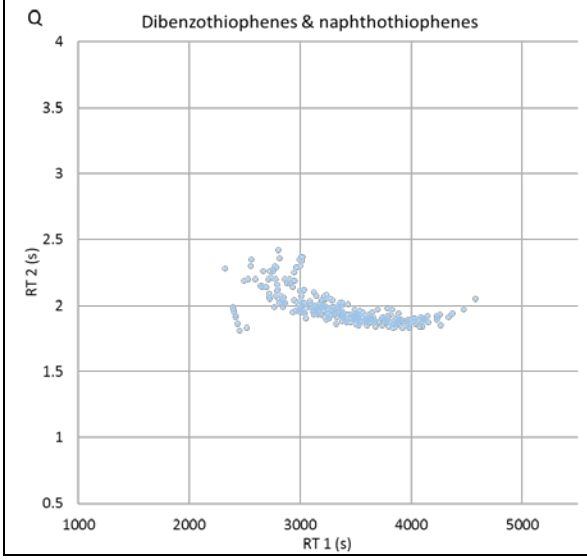	R 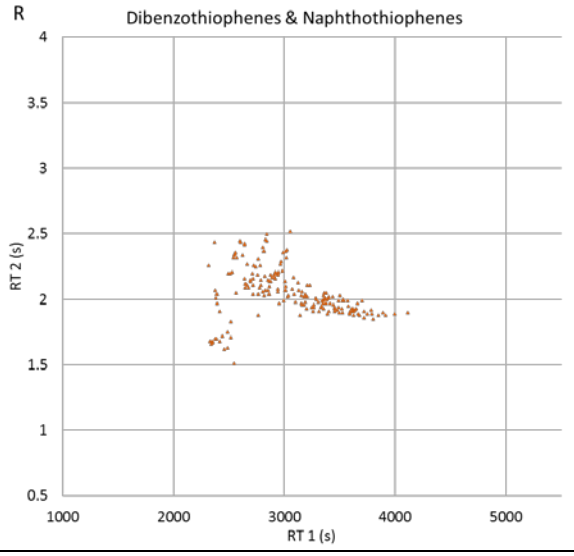

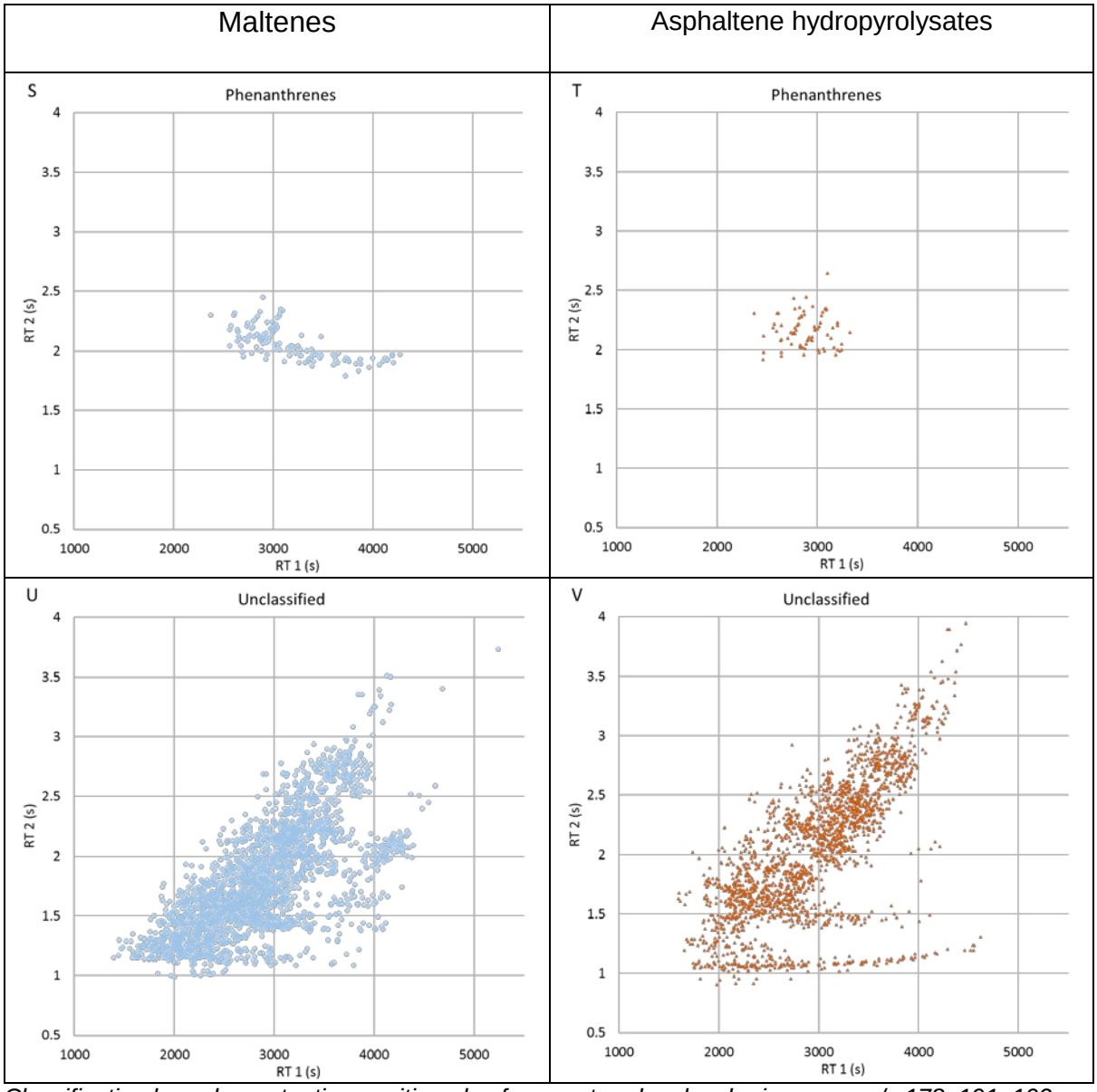

Classification based on retention position plus fragment and molecular ions e.g. m/z 178, 191, 192, 205, 206, 219, 220, 233, 234 = phenanthrenes.
Peaks classified as column bleed such as siloxanes not shown.

Figure S5 Elution positions of GC×GC-TOFMS chromatographic peaks of asphaltite 85 aromatic fraction classified by mass spectra into major compound groupings commonly found in oils (Fig. 1). Blue open circle (left column) = asphaltite maltenes. Orange triangle (right column) = asphaltene hydropyrolysates. RT1 = 1st dimension (volatility) retention time (s) and RT2 = 2nd dimension (polar) retention time (s).

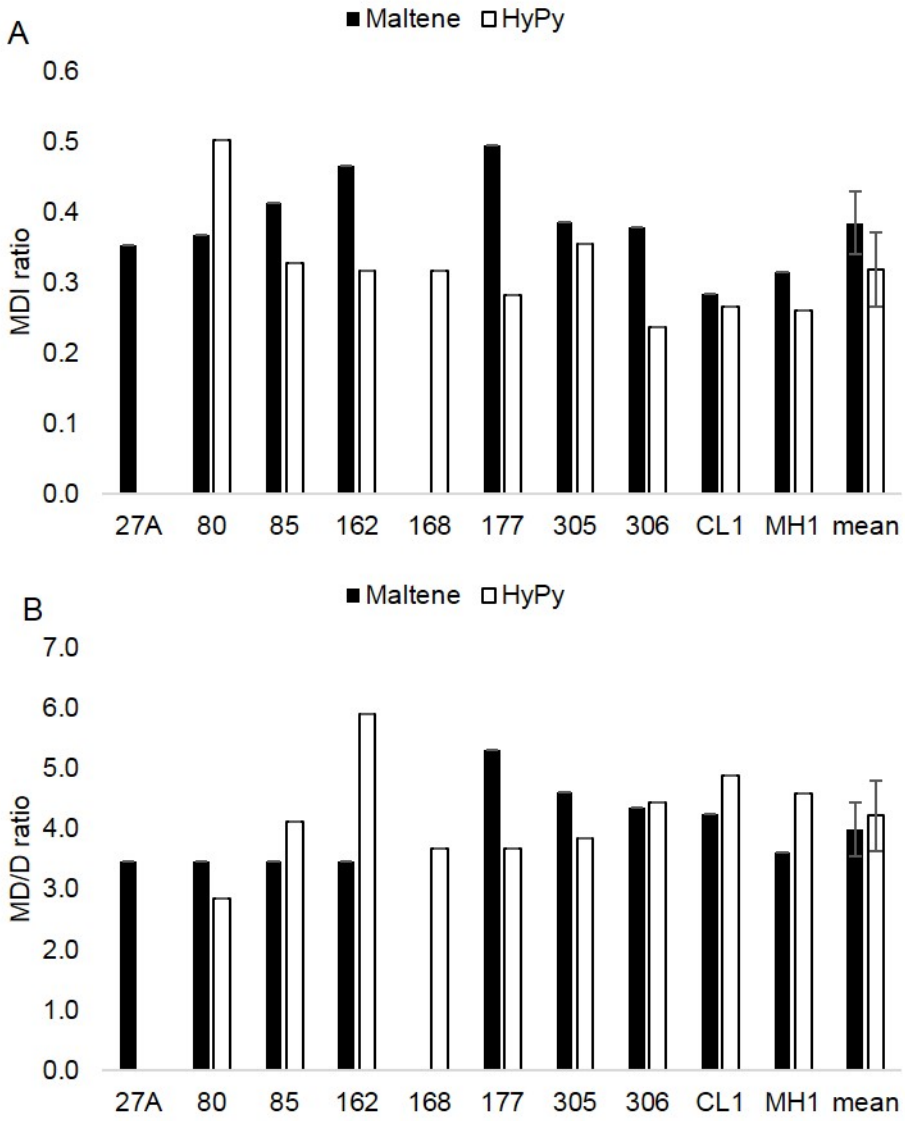

Fig. S6 Comparison of (A) Methyl Diamantane Index (MDI) and (B) Methyldiamantane/Diamantane (MD/D) in asphaltite maltenes and asphaltene hydropyrolysates (HyPy) analysed by GC×GC-TOFMS. Methyldiamantane peaks in 27A and 168 were below required signal to noise ratio. Mean ratios exclude missing data. Error bars show 95% confidence limits.

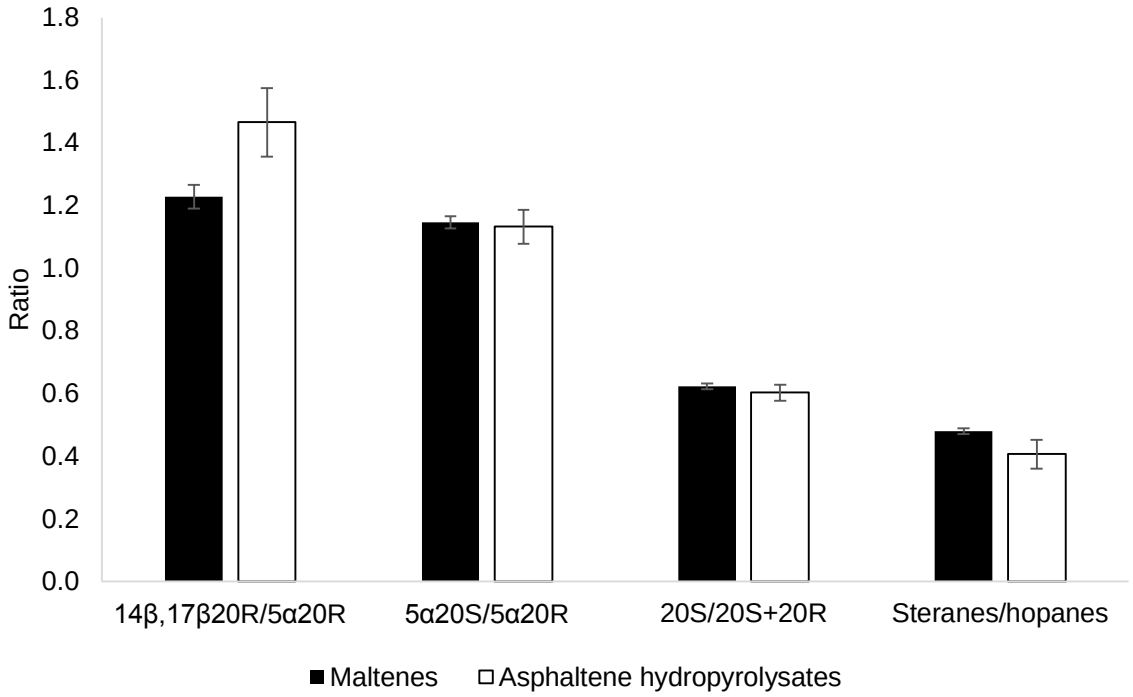

Fig S7 Sterane indices comparing asphaltite maltene saturates fraction with asphaltene hydropyrolysates. Error bars = standard deviation of the mean for all asphaltites.

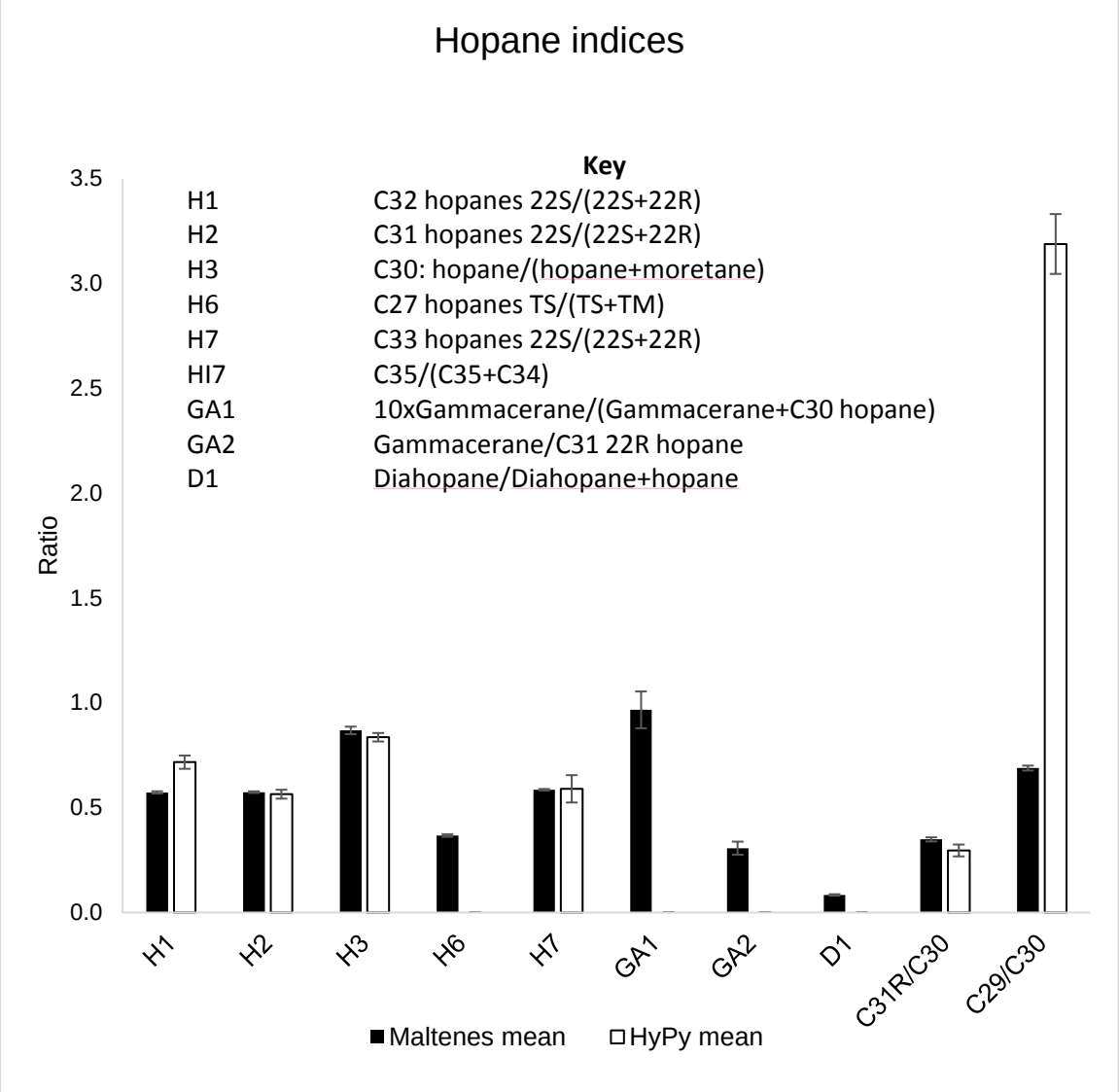

Fig. S8 Hopane indices comparing asphaltite maltene saturates fraction with asphaltene hydropyrolysates. Error bars = standard deviation of the mean for all asphaltites.

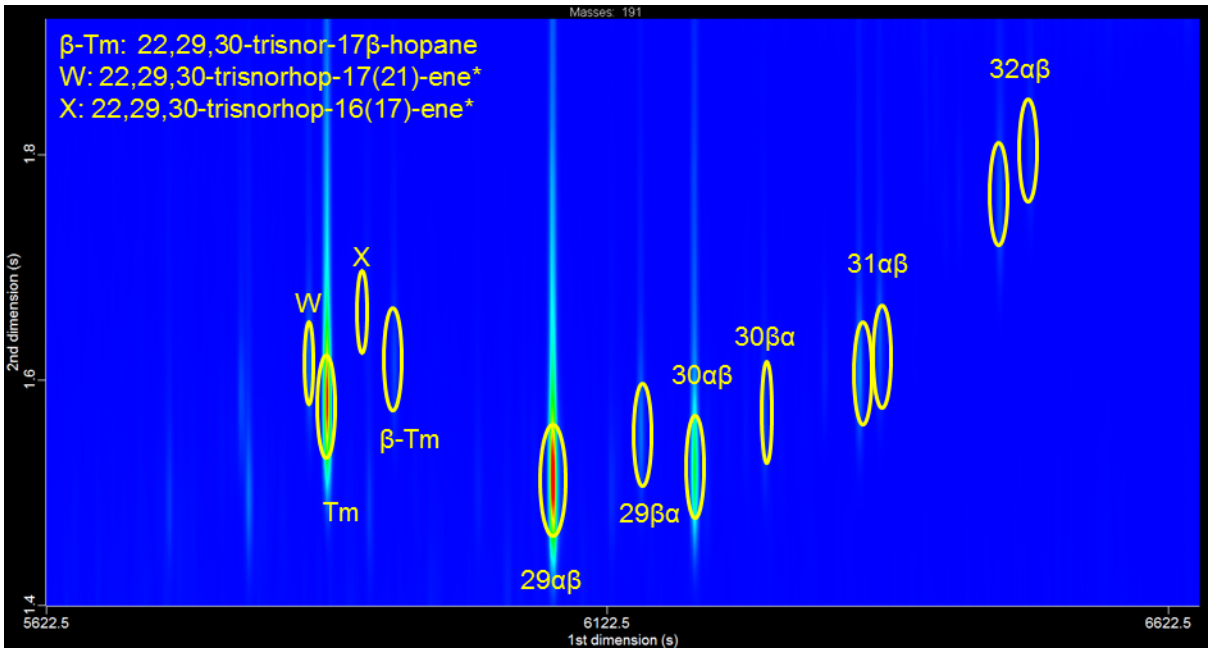

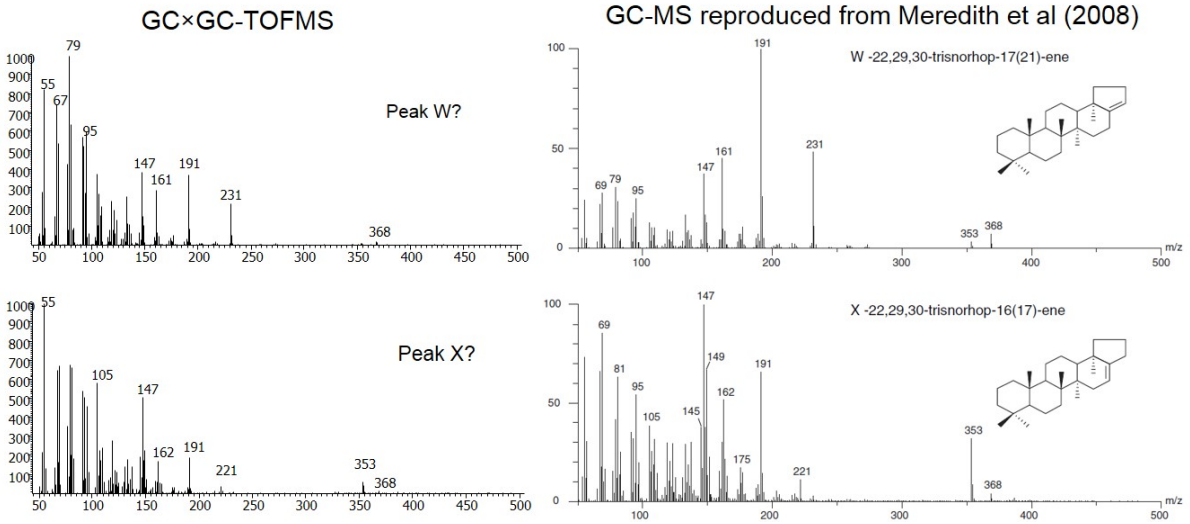

Fig S9 Tentatively assigned peaks W and X (top). GC×GC-TOFMS spectra of asphaltene 85 hydropyrolysates (left column) show reduced molecular and higher weight fragment ions but increased lower weight ions compared to GC-MS spectra reported by Meredith et al (2008).

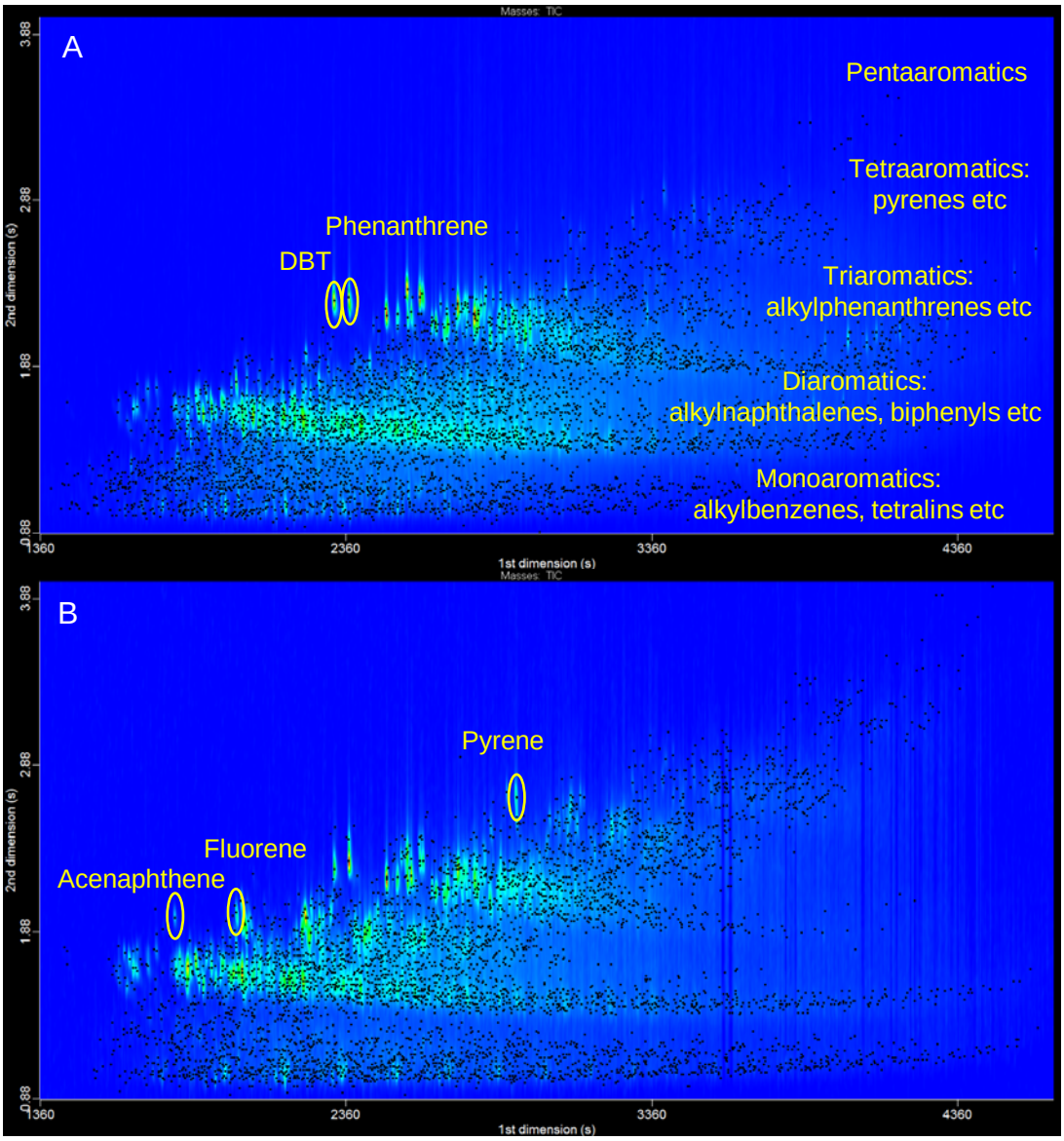

Fig. S10 GC×GC-TOFMS total ion chromatograms of aromatic fractions from (A) maltene and (B) asphaltene hydropyrolysates (asphaltite 85). Black dots indicate resolved peaks. Elution regions of increasing aromatic cyclicity with polarity indicated and some specific hydrocarbons and heterocyclic compounds shown.

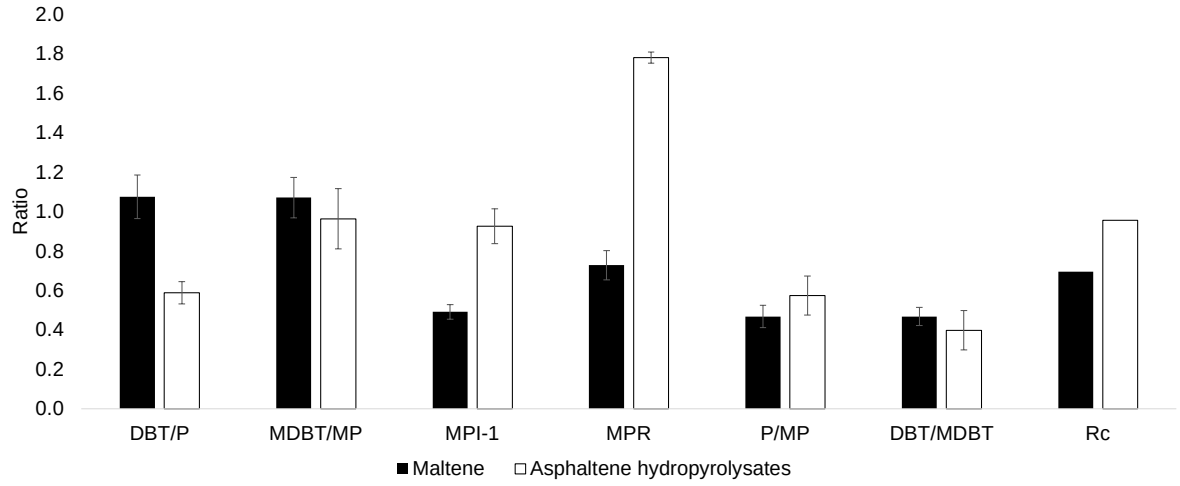

Fig. S11 Aromatic indices comparing asphaltite maltenes with asphaltene hydropyrolysates. Error bars = standard deviation of the mean for all asphaltites.

DBT = Dibenzothiophene

P = Phenanthrene

M = Methyl

MPI-1 = Methyl Phenanthrene Index = 1.5(2-MP + 3-MP)/(P + 1-MP + 9-MP)

MPR = Methyl Phenanthrene Ratio = 2-methylphenanthrene/1-methylphenanthrene

Rc = calculated vitrinite reflectance = 0.6*(MPI-1) + 0.4.

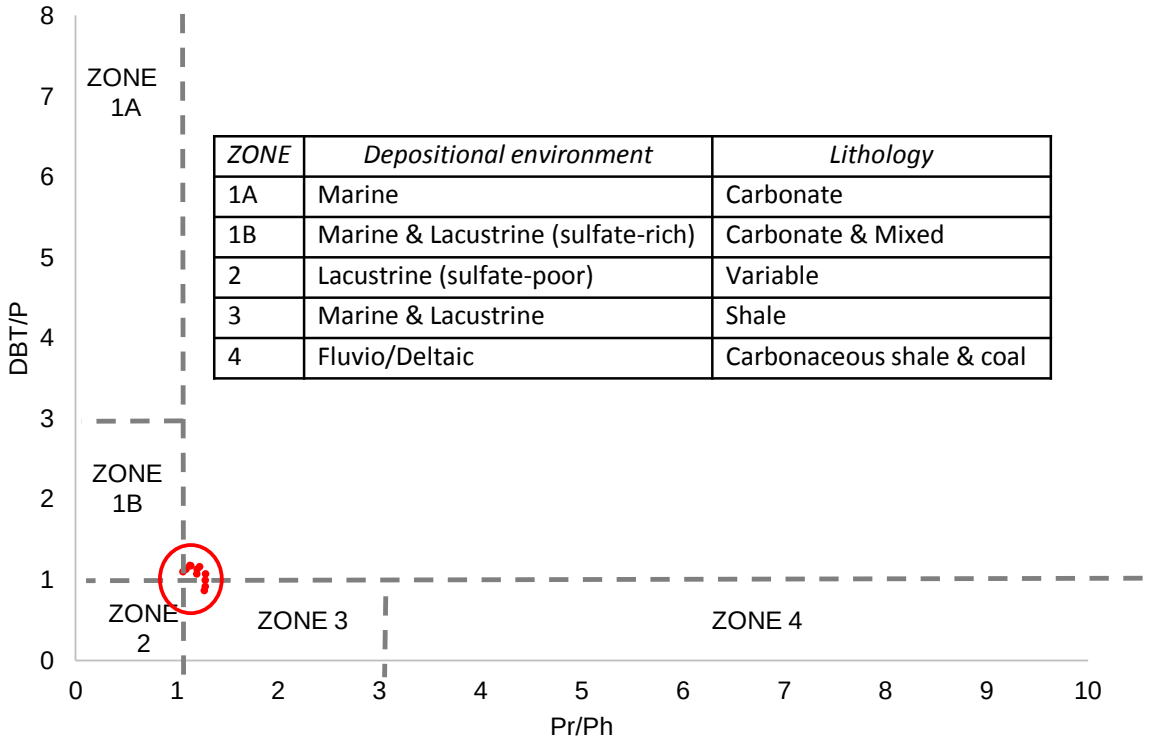

ZONE	*Depositional environment*	*Lithology*
1A	Marine	Carbonate
1B	Marine & Lacustrine (sulfate-rich)	Carbonate & Mixed
2	Lacustrine (sulfate-poor)	Variable
3	Marine & Lacustrine	Shale
4	Fluvio/Deltaic	Carbonaceous shale & coal

Fig. S12 Cross-plot of dibenzothiophene/phenanthrene ratio (DBT/Phen) to pristane/phytane ratio (Pr/Ph) showing zonal relationship with depositional environments and lithologies reported by Hughes et al (1995). Red circle highlights asphaltite plots.

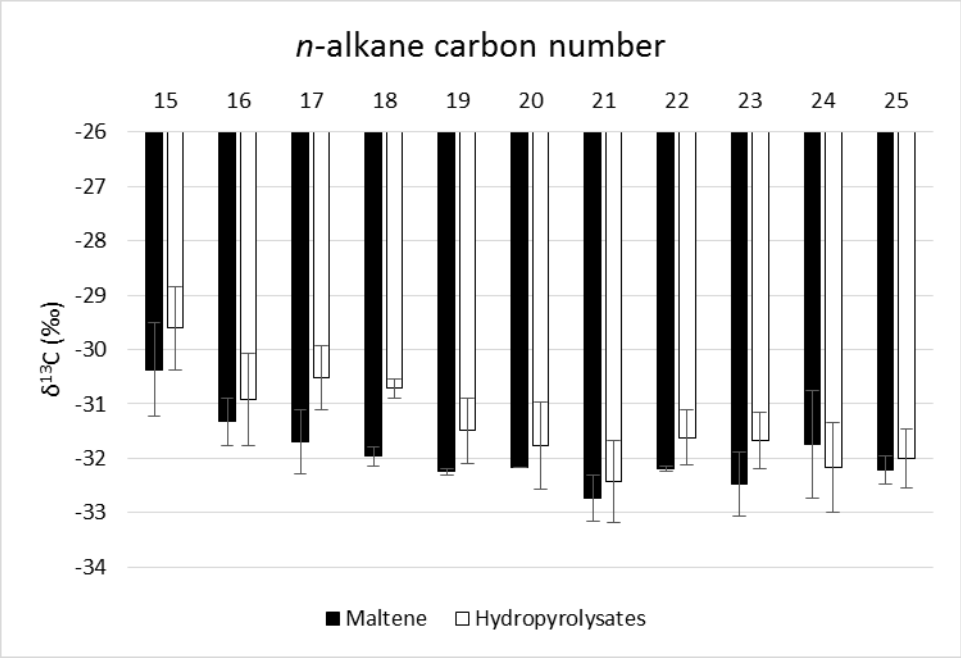

Fig. S13 Comparison of $\delta^{13}C$ (‰) values for *n*-alkanes (*n*-$C_{15\text{-}25}$) obtained from asphaltite 168 maltene and asphaltene hydropyrolysates. Error bars represent 95% confidence limits.

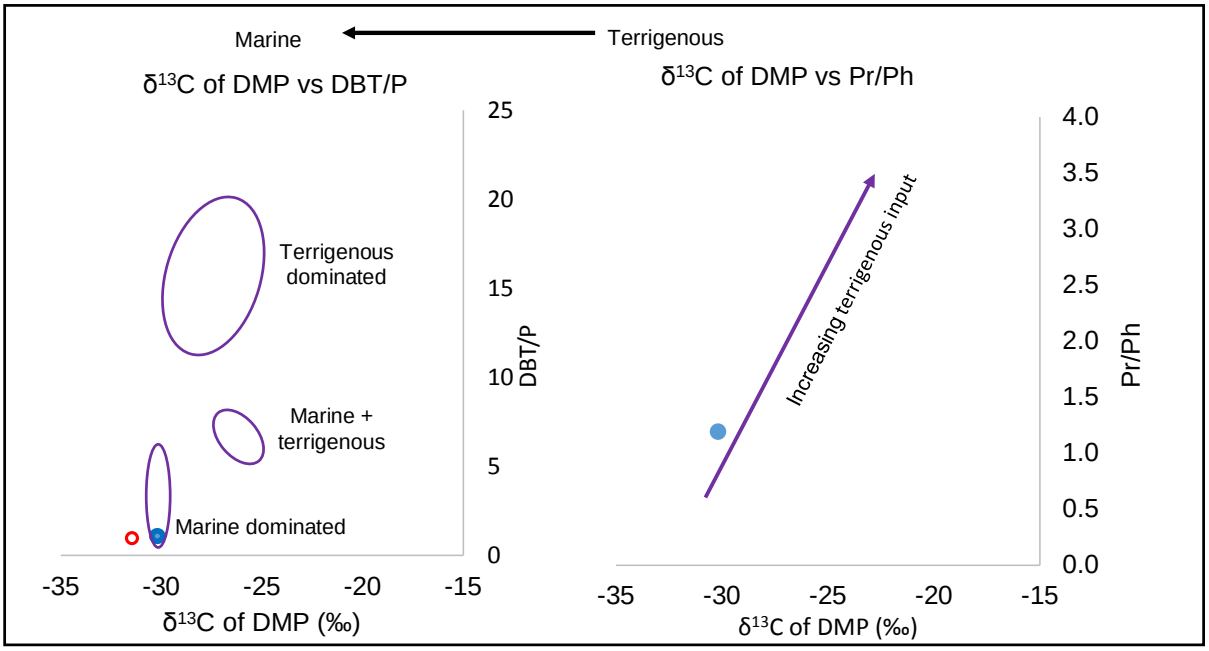

Fig. S14 Cross plot of mean dibenzothiophene/phenanthrene (DBT/P) and pristane/pristane (Pr/Ph) with mean $\delta^{13}C$ of dimethylphenanthrenes (DMP) for asphaltite maltenes (blue closed circle) and asphaltene hydropyrolysates (red open circle). Ellipses show approximate coordinates reported by Maslen et al (2011) for marine dominated, terrigenous dominated and mixed input.

References

Maslen, E., Grice, K., Le Metayer, P., Dawson, D., Edwards, D., 2011. Stable carbon isotopic compositions of individual aromatic hydrocarbons as source and age indicators in oils from western Australian basins. Organic Geochemistry 42, 387-398.

Meredith, W., Snape, C.E., Carr, A.D., Nytoft, H.P., Love, G.D., 2008. The occurrence of unusual hopenes in hydropyrolysates generated from severely biodegraded oil seep asphaltenes. Organic Geochemistry 39, 1243-1248.